The Dynamics of Warm and Cold Climates

D. RIND

Goddard Space Flight Center, Institute for Space Studies, New York, NY 10025

(Manuscript received and in final form 14 February 1985)

ABSTRACT

The atmospheric dynamics of five different climate simulations with the GISS GCM are compared to investigate the changes that occur as climate warms or cools. There are two ice age simulations, the current and doubled CO_2 climates, and a simulation of the warm Cretaceous. These climates have a range of global average surface air temperature of 13°C. The results are compared with those of other models, as well as to paleoclimate and recent observations.

The study shows that many zonally averaged processes do not change systematically as climate changes. In particular, the January Hadley cell, jet stream, mean precipitation patterns and total atmospheric transport show surprisingly little variation among the different climate simulations. While eddy energy increases as climate cools, the effective eddy forcing of the mean zonal wind and temperature fields is not significantly greater. All these features result from balances between competing factors, and while individual processes differ in the cold and warm climates, there is much compensation.

Additional results show that the relative humidity remains fairly constant as climate changes. The ratio of stationary to transient eddy kinetic energy also remains relatively constant. Eddy energy transports increase in colder climates, primarily due to changes in the stationary eddy transports. Cloud cover decreases as climate warms due to decreases in low-level clouds. The lapse rate in all the simulations follows the moist adiabatic value at low latitudes, and is close to the critical baroclinic adjustment value at upper midlatitudes. The latitudinal temperature gradients at midlatitudes of both the sea surface temperature and the vertically integrated air temperature are very similar in the diverse climates. It is speculated that this is due to the properties of the water molecule, and is the cause for much of the observed compensation.

1. Introduction

In addition to their use as a tool for modeling and studying atmospheric dynamics, general circulation models are increasingly being used to study past and future climates. The climate at the peak of the last ice age (18,000 years ago) has been simulated by several different modeling groups (e.g., Williams et al., 1974; Gates, 1976; Manabe and Hahn, 1977; Hansen et al., 1984; Manabe and Broccoli, 1984). Simulations of the Cretaceous climate (occurring about 60 million years ago) have been made by Baron and Washington (1982a,b, 1984) and Kuhn (1982). Kutzbach and Guetter (1984) have performed several experiments with a model using orbital parameters for different times, including 9000 and 6000 years ago. And simulations of the climate with doubled atmospheric CO_2 have become the benchmark for model intercomparison (e.g., Manabe and Wetherald, 1975, 1980; Hansen et al., 1984; Washington and Meehl, 1984).

These experiments represent a wide range of atmospheric and boundary conditions, and could be used to determine how the atmospheric general circulation varies as climate changes. There is good reason to suppose that substantial changes should exist. If warm climates have reduced latitudinal temperature gradients, quasi-geostrophic theory indicates the baroclinic instability and eddy energy should decrease, with a shift in instability toward shorter wavelengths (e.g., Green, 1960). Observations during historical warm periods show a tendency for a poleward shift of the upper level westerlies with a high circulation index (Lamb, 1972; Winstanley, 1973). The droughts experienced during the relatively warm period in the 1930s lead to the inference that the Hadley circulation might expand as climate warms (Budyko, 1974). If distinct dynamical changes do accompany climate change, general circulation models could be used to examine them.

However, the changes in circulation computed by the different models have not always been consistent. For example, Williams et al. (1974) and Gates (1976) found weaker Hadley circulations during July in their ice age simulations, while Manabe and Hahn (1977) reported a strengthened Hadley cell. Determining the reasons for differences between models is a very complicated and time consuming task, given the myriad of parameterizations incorporated into each model's structure.

In this study we will report how one particular model reacts when subject to different climatic and boundary conditions. We will compare the results with expectations such as those noted above, and with the results of other models. The answers given represent the perspective of a single GCM. Given the lack of substantial

model intercomparisons, it would be premature to generalize to other models or the atmosphere. Insofar as the model is capable of simulating the current and altered climates in a reasonable manner, it may further our understanding of the differences in atmospheric processes between warm and cold climates.

2. Model and experiments

The global climate model used for these experiments is that described in Hansen et al., (1983a) for the current climate. Despite the relatively coarse resolution (8° lat, 10° long) the model produces a reasonably accurate climate simulation, comparable to that of the several other models (see also Schlesinger, 1984). It has been used in a variety of climate and dynamics studies (e.g., Rind, 1982; Druyan, 1982; Miller et al., 1983; Henderson-Sellers and Gornitz, 1984; Chervin and Druyan, 1984; Hansen et al., 1984).

The main deficiencies in the January simulation relevant to this study are the following:

1) Excess rainfall occurs at 12°N (primarily in the Bay of Bengal).
2) The Hadley cell extends one grid box (8° lat) too far poleward.
3) The Ferrel cell is too weak (by about a factor of 3).
4) There is probably too much energy in wavenumbers 4–6 compared with wavenumbers 1–3.
5) The synoptic features at the surface move too slowly.

It is not known how these problems, or the choice of specific parameterizations (e.g., convection), affect the results. Problems 2–5 largely disappear with finer horizontal resolution (4° × 5°) (see Hansen et al., 1983a), and a comparison of two of the experiments (current climate and doubled CO_2) run with the finer resolution gave similar changes to those reported here. Model simulated and observed values of different variables from the current climate are given in Table 3.

Many of the expectations result from paleoclimate interpretations. This constrains us to use as accurate a portrayal of warm and cold climates as is possible. Rather than simply altering the ocean temperatures progressively, we will use the paleoclimate reconstructions of the sea surface temperatures. In addition, when the climate cools sufficiently, glaciers grow in the Northern Hemisphere and sea ice increases, changes which will also affect the dynamics. The cold climate simulations must have realistic boundary conditions in all respects for the comparisons with expectations based on paleoclimate observations to be meaningful. For the warm climates we will use the doubled atmospheric CO_2 experiment and a simulation of the Cretaceous climate. The climate runs, thus, involve differences in more than just global mean temperatures, and the other changes (e.g., topography) must be included in the analysis. The advantages of this heterogeneous set are 1) that it represents, at least in the model perspective, real climates; and 2) understandings arrived at from this variety of experiments are more likely to prove valid in other simulations.

The following are the experiments which will be compared:

1) *The current climate control run.* This run uses specified sea surface temperatures based on climatology. The climate simulation is that shown in Hansen et al., (1983a) for model II. The model was run for 6 years, and the results shown are for the last 5.

2) *The 18 k BP (18,000 years before present)* last glacial maximum run (Ice Age I). Model II has been run with the CLIMAP (1981) 18 k boundary conditions, including the earth's orbital parameters for that time (Berger, 1978). This run was also for 6 years, with the results averaged over the last 5. The resulting climate simulation has been previously discussed by Hansen et al. (1984) and Rind and Peteet (1985).

3) *Last glacial maximum with the CLIMAP (1981) sea surface temperatures reduced by 2°C (Ice Age II).* Comparison of the Ice Age I generated climate with land evidence of tropical climate during the last ice age has raised the possibility that CLIMAP data sets overestimate the sea surface temperatures, especially at low and subtropical latitudes (Rind and Peteet, 1985). A run with the sea surface temperatures reduced below CLIMAP values by 2°C everywhere was much more successful in reproducing the low latitude terrestrial data. As the global climate in this run is 2°C colder than that for the first ice age experiment, it provides an alternate cold climate scenario (and illustrates the effect of simply varying the ocean temperatures). The run was for 6 years, with the results reported for the last 5. This run has been discussed briefly by Hansen et al. (1984) and Rind and Peteet (1985).

4) *Doubled CO_2.* The control run can be used in a mode with specified ocean transports which approximately reproduce the observed sea surface temperatures under current conditions yet allow the ocean temperatures to change due to changes in thermal forcing at the surface. This mode has been used for an integration with doubled CO_2. Results have been reported by Hansen et al. (1984). As the sea surface temperatures are calculated, not prescribed, it was necessary to integrate this simulation for 35 years to reach equilibrium. The results reported here are for the last 10 years.

5) *Sixty-five million year BP climate simulation (Mesozoic).* This run is an attempt to simulate the climate at the end of the Cretaceous while conditions were still warm but continents had moved closer to their current positions than they had been earlier in time. The initial run of this model has been reported by Kuhn (1982), although the actual run discussed here, with modified boundary conditions, was made by Fleming (1983). Sea surface temperatures come from a variety

of sources (e.g., Frakes, 1979) although the maps by Fairbridge (shown by Kuhn, 1982) are the primary guides for the global patterns. Paleogeographic reconstruction comes primarily from Barron et al. (1981) with topography and vegetation from Fairbridge (in Kuhn, 1982). It should be emphasized that the boundary conditions for this run are very uncertain. The model was integrated for 3 years, with the results given here for the last 2.

These five experiments provide a range of global mean temperatures of 13°C. The two ice age experiments and the Mesozoic experiment have different topography from that of the current and doubled CO_2 experiments, and also somewhat different land distribution (especially in the Mesozoic; the ice age experiments have 4% more land exposed due to the reduction in sea level). The current and doubled CO_2 climate runs have the same ocean heat transport (implied in the case of the current climate), while the specified sea surface temperatures for the other runs means that their implied ocean heat transports differed. These distinctions will have to be included in the discussion of total heat transport. As a group, the experiments provide a challenging test of any generalizations of the differences between warm and cold climates.

3. Results

The model results are presented as responses to a series of questions. Global average values for specific variables are given in Table 1. Standard deviations of the variables from the five year current climate control run are given in Table 2. The changes explicitly discussed are those larger than several standard deviations from the control run. A comparison of the model simulation with observations for the current climate is given in Table 3.

Most of the figures will be in the form of zonal averages, with results from the five different experiments indicated on the same graph. While investigations of the current climate now concentrate on three-dimensional statistics (e.g., Lau and Oort, 1981), the simpler approach is useful for a first discussion of other climates.

Although all experiments march through the annual cycle, our discussion will be mainly of the January simulations. Many of the expectations result from paleoclimate observations in the Northern Hemisphere, and January presents the most active dynamic period for the Northern Hemisphere; the Southern Hemisphere in summer will be discussed but with less emphasis. We will comment briefly on the simulations for August at the end of this section. The results shown are for five Januarys for the current climate and each ice age simulation, ten Januarys for the doubled CO_2 run, and two for the Mesozoic (the two both showing the same general patterns). The January results are representative of the December through February simulations.

a. Temperature

• *Question 1:* Is it true that the temperature difference between warm and cold climates is greater at high latitudes?

This expectation arises from various sources. Paleoclimate sea surface temperature reconstructions tend to indicate only small changes in tropical and subtropical ocean temperatures (CLIMAP, 1981). Modeling studies (e.g., Manabe and Wetherald, 1975) have shown a large amplification at high latitudes. And observations (see Fig. 1 of Hansen et al., 1983b) show that the historical temperature variations at high latitudes, at least in the Northern Hemisphere, have been several times the global mean. As climate warms, high latitudes will have the greatest reductions in snow cover and sea ice, allowing more solar radiation to be absorbed. While the highest latitudes receive no sunlight in winter, they will get more heat from the ocean if sea ice diminishes. Furthermore, the high static stability of the winter lower troposphere traps added heat at low levels. In the equatorial region, excess heat will go into evaporating water instead of raising the sea surface temperature (Newell and Dopplick, 1979) and convection will tend to remove heat from the surface (Lindzen et al., 1982).

The model does show the high latitude amplification in the winter hemisphere (Fig. 1). As indicated in Table 1, the range of global average surface temperatures from Ice Age II to the Mesozoic is 12.9°C. At low latitudes the range is 7°C (with the doubled CO_2 being the warmest). At high winter latitudes it is about 40°C and at high summer latitudes about 20°C, although only 10°C excluding the Mesozoic. The strong temperature increase at 82°S in the Mesozoic is due to the appearance of snow-free land.

However, the answer to this question is strongly biased by the observations that produce the expectation. The sea surface temperatures (Fig. 1b) are prescribed except for the doubled CO_2 experiment. The high latitude amplification is built into the prescription. While that does not disqualify the results, assuming the prescription is accurate, it means that the model in most cases is not producing an independent result. The only true test is the change produced by the doubled CO_2 experiment since ocean temperatures are computed (although the ocean transports are specified). Comparing this run with the current climate simulation (Fig. 1a) it can be seen that the high latitude amplification is confined to the highest winter latitudes. The question of the magnitude of the real high latitude amplification is discussed in Hansen et al. (1984), who note that due to the convection, cloud feedback and ocean transports in this model the amplification is less than that of Manabe and Stouffer (1980). As will be shown, this aspect of the doubled CO_2 simulation affects certain characteristics of its dynamics.

The Mesozoic sea surface temperature at the equator is close to or slightly colder than that of the present. This agrees with the estimates of Frakes (1979) and

TABLE 1. Global average (a–e) January values and (f) August values for the different climate simulations.

Climate variable	Ice Age II	Ice Age I	Current	$2 \times CO_2$	Mesozoic
a. Temperature					
Surface air temperature (°C)	6.3	8.4	11.8	17.0	19.2
Sea surface temperature (°C)	17.9	19.9	19.2	23.1	23.3
Vertically integrated air temperature (°C)	−26.4	−24.0	−22.9	−17.8	−17.3
b. Hydrologic cycle					
Precipitation (mm d^{-1})	2.8	3.0	3.1	3.5	3.6
Evaporation (mm d^{-1})	2.8	3.0	3.1	3.5	3.6
Evaporation (W m^{-2})	81.0	88.1	89.7	102.7	104.0
Sensible heat flux (W m^{-2})	26.0	24.8	24.5	20.4	21.1
Low-level clouds (%)	40.6	39.8	38.2	34.7	30.1
High-level clouds (%)	27.9	28.7	28.7	30.3	29.2
Total cloud cover (%)	54	54	53	52	48
Ground albedo (%)	15.8	15.4	12.2	10.9	7.6
Planetary albedo (%)	33.6	33.1	31.3	29.3	25.3
Solar radiation absorbed at ground (W m^{-2})	168	169	177	181	195
Relative humidity (%) at 959 mb	76	76	78	78	80
Relative humidity (%) at 633 mb	52	53	54	55	55
Relative humidity (%) at 321 mb	40	40	41	44	45
Moist convective heating (10^{14} W)	371	400	410	478	498
Moist convective cloud depth (mb)	378	384	385	409	436
c. General circulation					
Vertically integrated stream function (10^9 kg s^{-1})	−17	−15	−15	−13	−22
200 mb meridional wind (m s^{-1})	0.4	0.3	0.3	0.3	0.7
200 mb zonal wind (m s^{-1})	13.2	14.4	14.8	16.0	9.7
200 mb eddy poleward transport of angular momentum (10^{17} J)	40.6	37.3	30.7	39.2	19.2
200 mb divergence of E-P flux (10^{16} J)	−178	−251	−258	−259	−261
d. Eddy energy					
Tropospheric APE (10^{19} J)	483	477	362	348	178
Tropospheric zonal APE (10^{19} J)	346	346	269	266	146
Tropospheric eddy APE (10^{19} J)	137	131	93	82	32
Topography (m)	348	348	233	233	89
633 mb baroclinic eddy generation (W m^{-2})	0.62	0.59	0.49	0.42	0.25
Eddy kinetic energy (10^4 J m^{-2})	127	124	107	96	71
Transient eddy kinetic energy (10^4 J m^{-2})	91	91	78	69	52
Stationary eddy kinetic energy (10^4 J m^{-2})	36	32	28	27	19
Tropospheric lapse rate (°C km^{-1})	5.7	5.6	5.7	5.6	5.7
Moist adiabatic lapse rate (°C km^{-1})	7.4	7.2	7.0	6.4	6.4
Dynamic lapse rate (°C km^{-1})	6.5	6.5	6.6	6.5	7.9
e. Energy transports					
Poleward transport sensible heat by eddies (10^{14} W)	30.8	29.2	24.1	20.6	13.9
Poleward transport sensible heat by transient eddies (10^{14} W)	17.3	16.9	16.0	13.6	8.7
Poleward transport sensible heat by stationary eddies (10^{14} W)	13.5	12.4	8.1	7.0	5.2
Poleward transport latent heat by eddies (10^{14} W)	21.9	23.5	22.7	27.4	16.6
Poleward transport static energy by eddies (10^{14} W)	52.3	52.3	46.7	47.9	30.4
Atmospheric poleward transport static energy (10^{14} W)	66.9	68.8	61.4	65.5	37.1
f. August results					
Surface air temperature (°C)	9.0	11.1	14.9	19.9	21.3
Total cloud cover (%)	50.2	50.8	51.4	48.4	44.3
Relative humidity (%) at 633 mb	51.3	51.3	52.8	54.6	55.9
Eddy kinetic energy (10^4 J m^{-2})	100.5	100.8	91.3	78.6	62.9
Poleward transport static energy by eddies (10^{14} W)	39.5	42.1	36.6	36.1	26.0
Atmospheric poleward transport static energy (10^{14} W)	52.1	56.5	53.1	53.6	33.7

TABLE 2. January standard deviations from five years of the current climate run for different latitudes and the global average. N.A. indicates global average not available.

Climate variable	60°N	30°N	0°	30°S	60°S	Global
a. Temperature						
Surface air temperature (°C)	1.09	0.41	0.17	0.12	0.03	0.09
Vertically integrated air temperature (°C)	0.52	0.31	0.25	0.19	0.25	0.18
b. Hydrologic cycle						
Precicpitation (mm d^{-1})	0.2	0.2	0.6	0.2	0.1	0.03
Evaporation (mm d^{-1})	0.2	0.2	0.2	0.2	0.1	0.03
Evaporation (W m^{-2})	6.4	5.8	4.7	4.8	1.5	0.8
Sensible heat flux (W m^{-2})	6.1	2.0	0.9	2.4	0.7	0.5
Low-level clouds (%)	1.7	2.0	0.8	2.2	0.7	0.4
High-level clouds (%)	2.4	1.5	4.2	2.0	1.1	0.3
Total cloud cover (%)	1.7	1.8	3.9	1.8	0.5	0.45
Ground albedo (%)	0.7	0.7	0.1	0.2	0.1	0.09
Planetary albedo (%)	0.7	0.7	0.5	0.8	0.1	0.12
Solar radiation absorbed at ground (W m^{-2})	0.4	1.8	2.5	4.0	0.6	0.41
Relative humidity (%) at 959 mb	1.5	1.5	0.5	1.3	0.5	0.34
Relative humidity (%) at 633 mb	3.0	1.7	1.9	1.9	0.6	0.15
Relative humidity (%) at 321 mb	2.1	1.6	2.1	1.5	1.2	0.32
Moist convective heating (10^{14} W)	7.4	16.7	50.3	15.1	2.9	33.1
Moist convective cloud depth (mb)	9.1	12.2	36.1	23.5	12.2	5.3
c. General circulation						
Vertically integrated stream function (10^9 kg s^{-1})	4.8	3.3	7.3	5.8	1.1	1.1
200 mb meridional wind (m s^{-1})	0.07	0.06	0.23	0.06	0.02	0.03
Vertically integrated vertical velocity (10^{-5} mb s^{-1})	2.4	2.1	3.2	1.2	1.3	0.0
200 mb zonal wind (m s^{-1})	2.5	2.6	0.5	0.8	1.0	0.4
200 mb eddy poleward transport angular momentum (10^{17} J)	8.0	13.2	7.7	19.9	6.2	N.A.
200 mb divergence of E-P flux (10^{16} J)	113.4	120.3	89.4	92.4	72.0	51.5
d. Eddy energy						
633 mb baroclinic generation (10^{12} W)	2.67	8.44	1.90	0.92	0.56	13.7
Eddy kinetic energy (10^4 J m^{-2})	7.4	19.6	1.4	9.8	8.4	4.9
Stationary eddy kinetic energy (10^4 J m^{-2})	9.9	13.1	1.0	5.2	7.5	4.8
Tropospheric lapse rate (°C km^{-1})	0.09	0.03	0.03	0.04	0.04	0.03
Moist adiabatic lapse rate (°C km^{-1})	0.05	0.04	0.03	0.02	0.03	0.02
Dynamic lapse rate (°C km^{-1})	0.55	0.10	0.00	0.09	0.23	0.15
e. Energy transports						
Northward transport sensible heat by eddies (10^{14} W)	6.3	4.5	0.1	0.6	0.7	N.A.
Northward transport sensible heat by stationary eddies (10^{14} W)	6.2	3.1	0.2	1.5	0.7	N.A.
Northward transport latent heat by eddies (10^{14} W)	1.1	2.8	0.2	3.0	1.0	N.A.
Northward transport static energy by eddies (10^{14} W)	5.9	5.6	0.2	3.0	1.0	N.A.
Divergence of E-P flux (10^{17} J)	50.6	120.7	26.4	52.6	41.2	0.0
Atmospheric northward transport static energy (10^{14} W)	4.5	4.3	3.7	3.0	2.1	N.A.

with the simulation for 100 million years BP of Barron and Washington (1984). It can be contrasted with the extremely warm high-latitude sea surface temperatures for this run, prescribed to be consistent with the observation of no permanent ice at high latitudes at this time. The Mesozoic experiment represents the inverse of the doubled CO_2 run, with extreme high-latitude amplification.

Figure 1c gives the vertically integrated temperature, from the surface up to 10 mb. Away from the influence

TABLE 3. Comparison of model simulations and observations for January. Asterisk indicates the observations are for December–February.

Climate variable	Current climate model simulation	Observation	Reference
a. Horizontal temperature field			
Surface air temperature (°C) (global average)	11.8	12.2	(Schutz & Gates, 1971)
Sea surface temperature (°C) (global average)	19.2 (prescribed)	18.6	(Schutz & Gates, 1971)
Vertically integrated air temperature (°C) (global average)	−22.9	−21.2*	(Oort & Peixoto, 1983)
Surface air temperature change (°C) (27–67°N)	39.6	39.9	(Schutz & Gates, 1971)
Sea surface temperature change (°C) (27–67°N)	18.1 (prescribed)	17°.0	(Schutz & Gates, 1971)
Vertically integrated air temperature change (°C) (27–67°N)	19.0	18.5*	(Oort & Peixoto, 1983)
b. Hydrologic cycle			
Precipitation (mm d^{-1}) (global average)	3.1	2.9*	(Schutz & Gates, 1971)
Precipitation (mm d^{-1}) (12°N/27°N)	5.8/2.7	3.0*/2.0*	(Schutz & Gates, 1971)
Evaporation (mm d^{-1}) (global average)	3.1	3.1	(Schutz & Gates, 1971)
Sensible heat flux (1y d^{-1}) (global average)	50.6	35.7	(Schutz & Gates, 1971)
Total cloud cover (%) (N.H.)	54.3	56.2	(Schutz & Gates, 1971)
Planetary albedo (%) (global average)	31	31	(Stephens *et al.*, 1981)
Solar radiation absorbed at surface (1y d^{-1}) (global average)	365	377	(Schutz & Gates, 1971)
800 mb relative humidity (%) (global average)	61	58	
c. General circulation			
Hadley Cell peak intensity (10^9 kg s^{-1})	−142	−175	(Oort & Rasmusson, 1971)
Hadley Cell northern extent (°N lat.)	42	33	(Oort & Rasmusson, 1971)
Ferrel Cell peak intensity (10^9 kg s^{-1})	15	50	(Oort & Rasmusson, 1971)
Meridional wind (m s^{-1}) (16°N, 200 mb/850 mb)	2.6/−1.2	2.7/−1.0*	(Oort & Peixoto, 1983)
Vertically integrated vertical velocity (10^{-4} mb s^{-1}) (27°N/45°N)	1.3/0.3	1.4/−0.1*	(Oort & Peixoto, 1983)
Zonal wind (m s^{-1}) (30°N, 200 mb)	33.7	39.4*	(Oort & Peixoto, 1983)
Eddy transport angular momentum (m^2 s^{-2}) (30°N, 200 mb)	60.9	71.1*	(Oort & Peixoto, 1983)
d. Eddy energy			
Available potential energy (10^5 J m^{-2}) (Northern Hemisphere)	58.4	65.6*	(Oort & Peixoto, 1983)
EAPA → EKE (W m^{-2}) (Northern Hemisphere)	2.4	2.8*	(Oort & Peixoto, 1983)
EKE → ZKE (W m^{-2}) (Northern Hemisphere)	0.20	0.27*	(Oort & Peixoto, 1983)
Peak EKE (m^2 s^{-2}) (40°N, 300 mb)	307	305*	(Oort & Peixoto, 1983)
Peak stationary EKE (m^2 s^{-2}) (30°N, 200 mb)	10.9	8.7*	(Oort & Peixoto, 1983)
Peak transient EKE (m^2 s^{-2}) (45°N, 300 mb)	24.4	25.9*	(Oort & Peixoto, 1983)
EKE (10^5 J m^{-2}) (Northern Hemisphere)	13.5	8.8*	(Oort & Peixoto, 1983)
ZKE (10^5 J m^{-2}) (Northern Hemisphere)	8.6	8.0*	(Oort & Peixoto, 1983)
EKE ratio (wave no. 1–3/wave no. 4–6)	1.04	1.54*	(Saltzman, 1970)
500 mb trough positions (°W)	−135/80/25	−144/75/30	(Crutcher & Meserve, 1970)
Tropospheric lapse rate (°C km^{-1}) (global average)	5.7	5.7	(Oort & Peixoto, 1983)
e. Energy transports			
Peak eddy transport sensible heat (°C m s^{-1}) (50°N, 850 mb)	28.1	27.6*	(Oort & Peixoto, 1983)
Peak stationary eddy transport sensible heat (°C m s^{-1}) (50°N, 850 mb)	8.5	13.3*	(Oort & Peixoto, 1983)
Peak transient eddy transport sensible heat (°C m s^{-1}) (45°N, 850 mb)	19.6	15.4*	(Oort & Peixoto, 1983)
Peak eddy transport latent heat (g kg^{-1} m s^{-1}) (30°N, 1000 mb)	8.3	6.9*	(Oort & Peixoto, 1983)
Peak eddy transport energy (°C m s^{-1}) (45°N, 850 mb)	44.8	35.5*	(Oort & Peixoto, 1983)
Vertical integrated peak atmosphere transport energy (°C m s^{-1}) (50°N)	22.6	16.4*	(Oort & Peixoto, 1983)

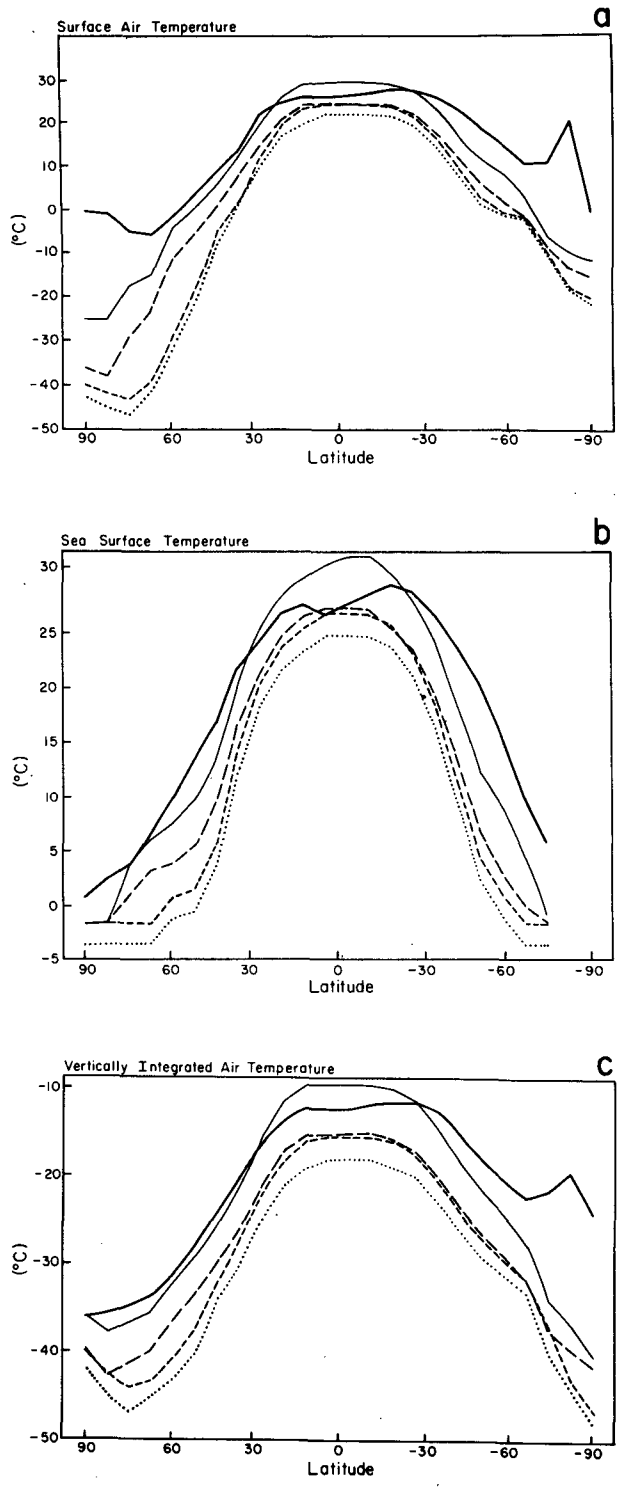

FIG. 1. General format for most of the figures: zonally averaged January value plotted as a function of latitude for the five different climates. Ice Age II: doted line; Ice Age I: short dashes; current climate: long dashes; doubled CO_2: thin solid line; Mesozoic: thick solid line. Thus the lines become more continuous and thicker as the climate warms. Shown in this figure are the results for (a) surface air temperature; (b) sea surface temperature; (c) vertically integrated air temperature, from the surface to 10 mb.

of the surface boundary conditions, and with the integration removing the effect of the different low altitude stabilities, the high-latitude amplification is considerably reduced or entirely eliminated. The vertically-integrated midlatitude temperature gradients are very similar in all the simulations for both winter hemispheres (Table 4). There is an apparent correspondence between the sea surface and vertically integrated temperature gradients, both for the experiments in which the sea surface temperature is specified, and the doubled CO_2 run where it is calculated although the numerical similarity depends upon the span of latitudes chosen. We will return to the possible implications of this correspondence in the discussion.

b. Hydrologic cycle

• *Question 2:* Do the latitudes of maximum precipitation shift systematically as the climate warms?

Paleoclimate observations of lake levels (Street and Grove, 1979) and sand dunes (Sarnthein, 1978) indicate that arid conditions prevailed in the tropics during the last ice age, while there was increased rainfall at the climatic optimum. Drier conditions occurred at midlatitudes of the Northern Hemisphere during the relatively warm decade of the 1930s and in the doubled CO_2 simulation of Manabe et al. (1975). Such changes may imply that shifts in mean vertical motion patterns occur when climate warms.

January results for precipitation (Fig. 2a) are representative of the annual results, which show there are no systematic shifts in the model from cold to warm climates. The rainfall pattern appears to depend strongly on the pattern of the sea surface temperatures. The current climate simulation has excessive precipitation at 12°N (in the Bay of Bengal primarily); in the ice age experiments, the warm subtropical Pacific Ocean provides moisture which is swept by the trade winds to the equator, shifting the precipitation maximum there. In the Mesozoic experiment, the relatively cool tropical sea surface temperatures (Fig. 1b) are associated with a precipitation minimum at 4°N. In the

TABLE 4. Temperature changes across midlatitudes.

	January 27–67°N		August 27–67°S	
	Δ Sea surface temperature (°C)	Δ Vertically integrated air temperature (°C)	Δ Sea surface temperature (°C)	Δ Vertically integrated air temperature (°C)
Ice Age II	22.0	21.0	20.1	19.2
Ice Age I	22.1	21.4	20.1	19.4
Current	18.1	19.0	20.7	19.0
$2 \times CO_2$	19.2	20.0	22.6	19.4
Mesozoic	17.9	17.6	15.9	14.6

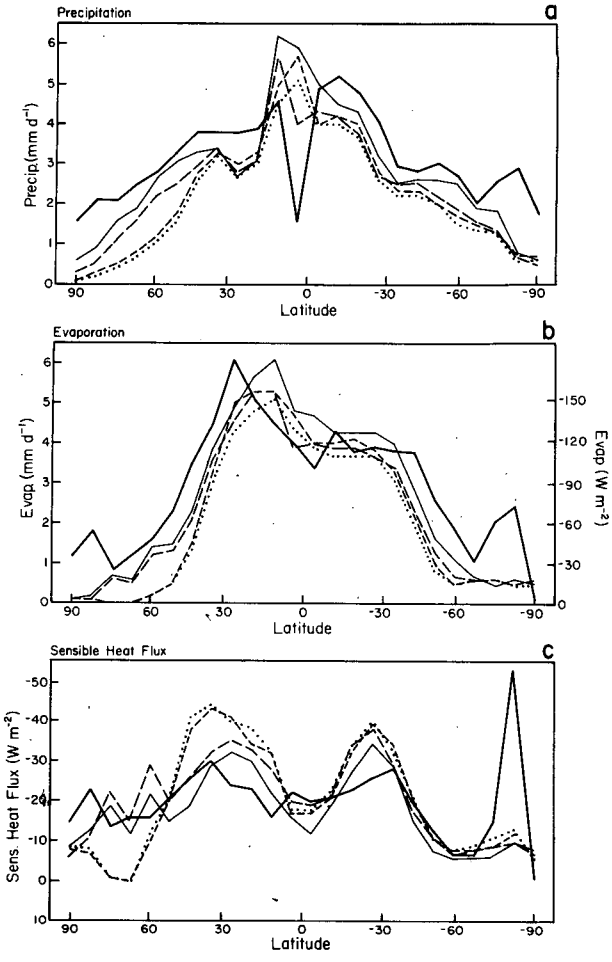

FIG. 2. As in Fig. 1 for (a) precipitation; (b) evaporation; (c) sensible heat flux.

other warm experiment, doubled CO_2, increased sea surface temperatures at the equator are associated with increased low-latitude precipitation. The region of precipitation minimum occurs in all cases at 27°N except for the Mesozoic. The only systematic effects seen are the global increase of precipitation from cold to warm climates, most apparent poleward of 40°N and 35°S. The warmer air can hold more moisture and the vertical stability decreases at the higher latitudes, allowing more moist convective precipitation.

The coarse grid of this model could not be expected to show small shifts in latitude which might have climatic importance. The results do emphasize that to determine what will happen to low-latitude precipitation, it is important to know what happens to the low- and subtropical-latitude sea surface temperature fields.

The influence of the sea surface temperatures on the hydrologic cycle can also be explored by noting their impact on evaporation (Fig. 2b) and sensible heat flux (Fig. 2c). The sensible heat flux at most locations is greater in the colder climates, while the latent heat flux is greater in the warmer climates. Reduced evaporation occurs in the Mesozoic equatorial region where the prescribed sea surface temperatures feature a relative minimum.

• *Question 3:* What happens to cloud cover as the climate warms?

Schneider et al. (1978) found that increased sea surface temperatures in a GCM experiment led to decreased global cloud cover, especially in the subtropics. There is, as yet, no convincing observational evidence to suggest how clouds react to climate change. Roads (1978) reviewed the difficulties inherent in trying to decide on a theoretical basis how wave generated clouds would be affected by climate warming.

The model results show that total cloud cover decreases as the climate warms. The total cloud cover change (Fig. 3c) is dominated by the change in low

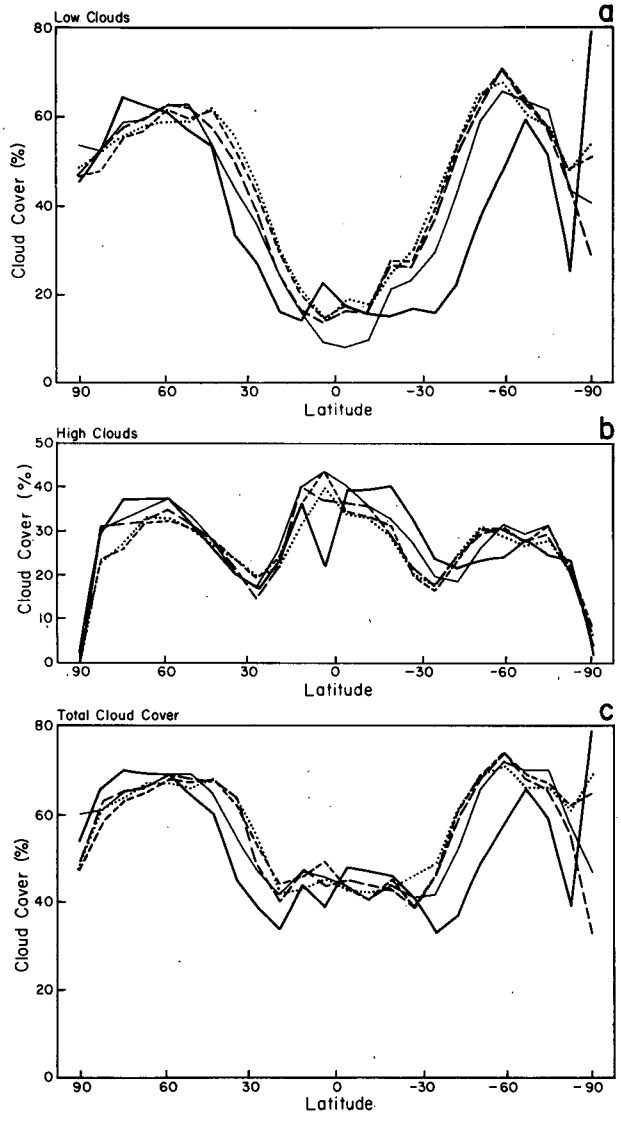

FIG. 3. As in Fig. 1 for (a) low level clouds (surface to 854 mb); (b) high level clouds (390–150 mb); (c) total cloud cover.

clouds (Fig. 3a), which decrease as the climate warms except at the lowest and highest latitudes. High clouds (Fig. 3b) tend to increase in the warmer climates at low and subtropical latitudes of the summer hemisphere, and from 50° poleward in the winter hemisphere. These cloud cover changes correlate with changes in the mean vertical motion (Fig. 6c). Where there is greater ascent, high clouds increase and low clouds (which are essentially in the planetary boundary layer) decrease; the reverse holds where there is greater descent. The vertical motion field affects both the large-scale distribution of moisture and convective cloud generation (for example, with greater large-scale descent, the altitude which is reached by convection is more limited and moisture is trapped in the boundary layer). The increase in low-level clouds at midlatitudes in the cold climates occurs over the oceans and appears to be associated with cold air coming off the continents. It also closely parallels the increase in eddy kinetic energy (Fig. 10a).

While the ability of GCMs to generate clouds realistically has yet to be fully tested, the results are not unreasonable; considerable boundary layer cloud cover is found today in regions of subsidence over the ocean. We also note that these results are in almost complete agreement with three other modeling studies: the change in cloud cover in the doubled CO_2 experiments of Washington and Meehl (1984) and Wetherald (personal communication, 1984), and the increases in low-level clouds in the ice age simulation of Williams et al. (1974). The NCAR and GFDL models used for these studies have completely different convection and cloud generation schemes from that employed here.

The reduction of low clouds and increase in high clouds in the $2 \times CO_2$ experiment tends to amplify the climate response, as discussed by Hansen et al. (1984). In addition to increasing the atmospheric greenhouse capacity, the changes affect the albedo. The planetary albedo (Fig. 4a) and the ground albedo (Fig. 4b) decrease as climate warms. The ground albedo decrease is due to the reductions in snow cover and sea ice. The planetary albedo change also includes the cloud cover changes, as the model's low clouds have larger albedos than do the high clouds. Both surface and atmospheric albedo processes are thus working in the same direction; however, the planetary albedo change is small in the Northern Hemisphere, much less than the change in ground albedo, because the atmospheric albedo change is relatively small. Thus the absorbed radiation (Fig. 4c) in this hemisphere is very similar in the different experiments, and does not contribute to high latitude temperature amplification.

• *Question 4:* Does the relative humidity remain constant as climate changes?

This question is instigated by the assumption initially offered by Manabe and Wetherald (1967) that in a one-dimensional radiative-convective model it is better to fix the relative humidity in a climate change experiment

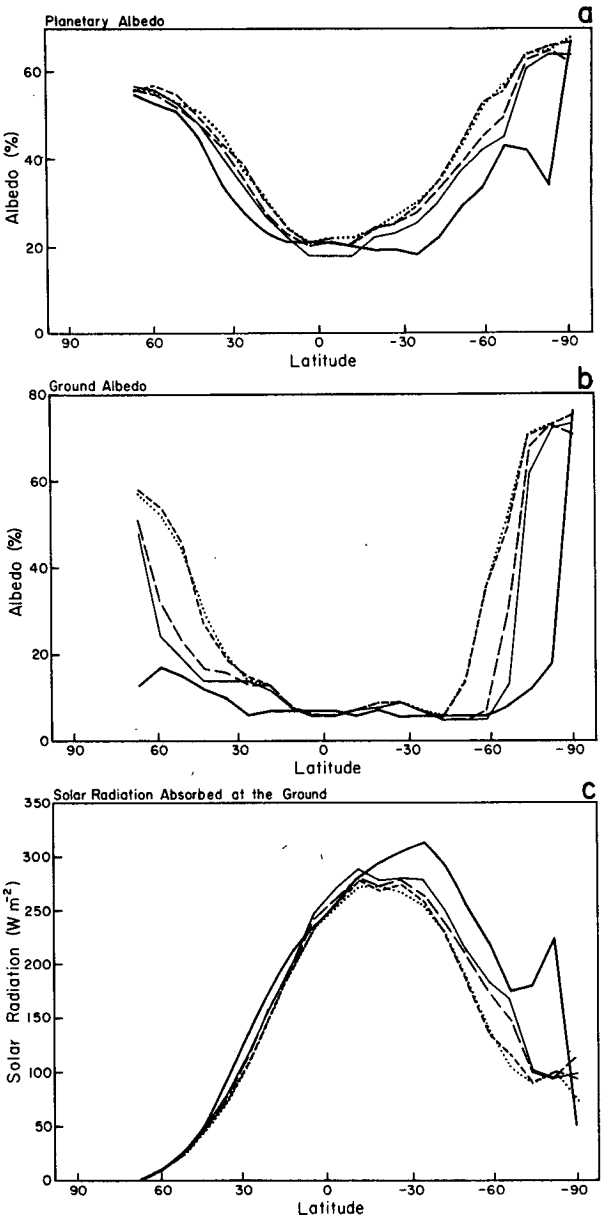

FIG. 4. As in Fig. 1 for (a) planetary albedo; (b) ground albedo; (c) solar radiation absorbed at the ground. The albedo values are undefined north of the Arctic Circle where there is no solar radiation.

than to fix the specific humidity. As proof of this, they referred to the difference in relative and specific humidities between summer and winter. The summer relative humidity is similar to that in winter, being slightly greater at mid- and upper-tropospheric levels, while the specific humidity varies greatly. The invariance of relative humidity is now a standard assumption in radiative-convective models.

The global average relative humidity is fairly constant in these experiments. It increases between 5 and 10% (with the higher amounts at the highest troposphere levels) between Ice Age II and Mesozoic exper-

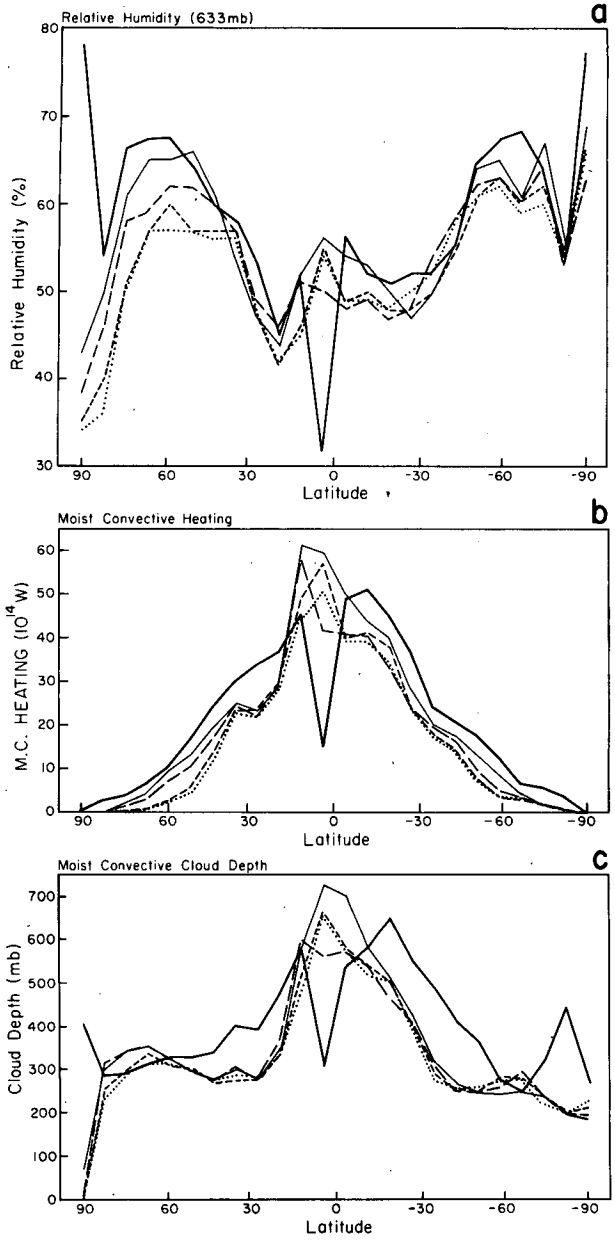

FIG. 5. As in Fig. 1 for (a) relative humidity at 633 mb; (b) vertically averaged moist convective heating; (c) moist convective cloud depth.

iments (Table 1). In the midtroposphere (Fig. 5a), an increase in relative humidity as climate warms occurs at mid- and upper-latitudes in both hemispheres, with a difference of about 10% at 60°N. Changes are smaller and less systematic at low and subtropical latitudes, which dominate the global average. The strong decrease in relative humidity at 4°N in the Mesozoic experiment is apparently connected with the relative minimum in sea surface temperatures. We note that the general trend of relative humidity from cold to warm climates is similar to that from winter to summer, although the seasonal change is greater at low and subtropical latitudes (London, 1957).

• *Question 5:* Does convection increase as the climate warms?

Convection is generated by moist static instability; with warmer sea surface temperatures and increased evaporation, this instability should increase. The association of convection and warm ocean waters has been verified by observations of greatest convective penetration near Indonesia (Newell and Gould-Stewart, 1981).

The model results show that heating by moist convection (Fig. 5b) and convective penetration (Fig. 5c) are greater when sea surface temperatures are very warm (CO_2 experiment near the equator, Mesozoic at most other latitudes). The active equatorial convection in the ice age experiments arises in part from the relatively warm subtropical gyres in the CLIMAP reconstruction which feed moisture into cold air being swept by the trade winds toward the equator. In contrast, the Mesozoic run has reduced equatorial convection. Moist static instability is influenced by sea surface temperature gradients, rather than simply by the absolute sea surface temperature magnitude, as these examples illustrate.

c. *General circulation*

• *Question 6:* Does the Hadley cell shift poleward as the climate warms?

This question is suggested by the same types of observations noted in question 2 for shift of precipitation regions. In addition, there have been numerous studies of current climate analogs, warm and cold periods, which show high circulation index (poleward shift of westerlies) during warmer periods, and low circulation index, or expanded and weakened westerlies, during colder periods (e.g., Lamb, 1972; Winstanley, 1973). Increased Hadley cell extent should accompany higher convective penetration according to the suggestion of Held and Hou (1980).

The model does not show a systematic poleward shift of the circulation cells as the climate warms. The Hadley cell is defined by the negative stream function (vertically integrated, Fig. 6a), and characterized by a northward upper troposphere meridional wind (Fig. 6b), with upward vertical velocity at its southern limit and downward vertical velocity for its poleward extension (Fig. 6c). Except for the Mesozoic run, the experiments show a small but consistent shift toward expanded Hadley circulation for the colder climates. The differences are at best only marginally significant (Table 2). The Cretaceous simulation of Barron and Washington (1982b) also showed little poleward shift of the Hadley cell. The zonal mean thermodynamic energy equation can be written:

$$\frac{\partial\bar{\theta}}{\partial t} = \bar{Q} + \left[-\frac{\partial(\bar{\theta}\cos\phi)}{a\cos\phi\partial\phi}\bar{v} - \frac{\partial\bar{\theta}}{\partial p}\bar{\omega}\right] + \left[-\frac{\partial(\overline{v'\theta'}\cos^2\phi)}{a\cos^3\phi\partial\phi} - \frac{\partial}{\partial p}(\overline{\omega'\theta'})\right], \quad (1)$$

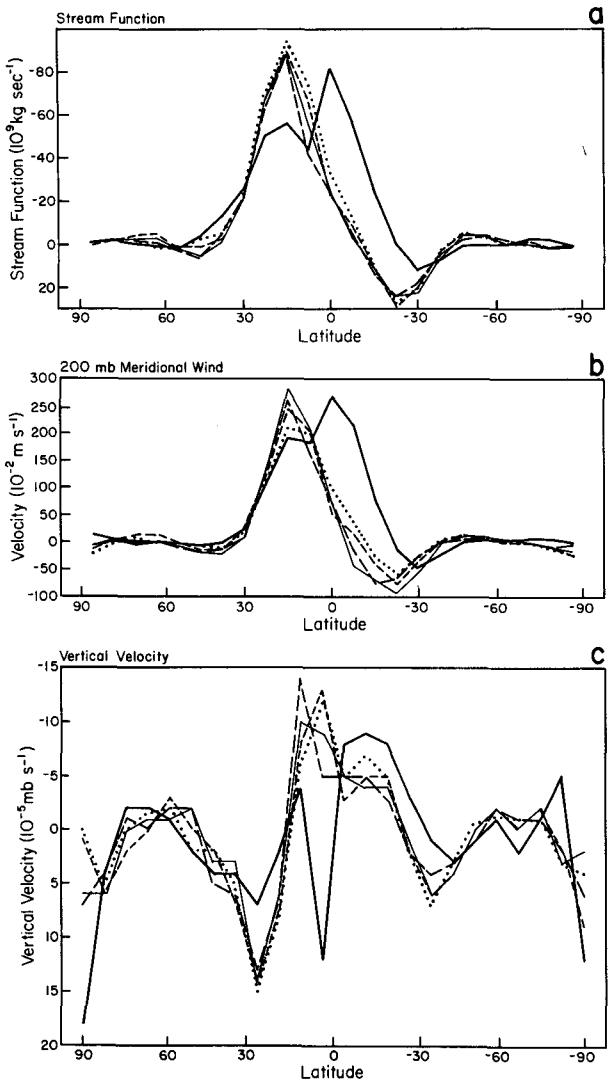

FIG. 6. As in Fig. 1 for (a) vertically integrated streamfunction; (b) 200 mb meridional wind; (c) vertically integrated vertical velocity.

where θ is the potential temperature, v and ω the meridional and vertical velocities, respectively, in constant pressure coordinates, ϕ the latitude, a the earth's radius, the overbar represents the zonal mean and the prime the deviation from the zonal mean; $\bar{Q}$ is the zonal mean heating rate, the first bracketed term represents heating associated with the mean circulation, and the second bracketed term gives the heat convergence by eddies. The heating rate may be broken down into its components:

$$\bar{Q} = \bar{Q}_{LW} + \bar{Q}_{SW} + \bar{Q}_{Shf} + \bar{Q}_{mc} + \bar{Q}_{Lsc} + \bar{Q}_{dc}, \quad (2)$$

where the terms represent, respectively, long wave cooling and short wave heating, sensible heat flux from the surface, moist convective heating, large-scale condensation heating, and the effect of dry convection.

The vertically integrated values for the different terms in equations (1) and (2) are given in Table 5 for 43°N and 51°N. The vertical integration eliminates the effect of dry convection and the vertical eddy convergence, and reduces the moist convective heating to its latent heat release component. In the warmer climates most of the heating is associated with moist convection (which may occur as part of storm-generated precipitation) with much of the moisture provided by local evaporation off the warm ocean. In the colder climates dynamic heat and moisture transports, large-scale condensation, and sensible heat fluxes become increasingly important. All terms are calculated accurately by the model, and the balance in all the experiments is satisfied to better than 0.1°C day^{-1}. Note that subsidence occurs in all the experiments at 43°N, and the changes at 51°N are, at best, of marginal significance.

The results emphasize that warm and cold climates have different mechanisms for heating the atmosphere, all do not change in the same direction as climate changes, and the compensations work to limit the change in total heating and the change in the latitudinal

TABLE 5. Vertical velocity and vertically integrated heating rates (°C d^{-1}) at 43° and 51°N. For explanation of symbols see Eqs. (1) and (2).

Experiment	ω (10^{-5} mb s^{-1})	$\frac{\partial\theta}{\partial t}$	Q_{LW}	Q_{SW}	Q_{Shf}	Q_{mc}	Q_{Lsc}	Mean cell horizontal	Mean cell vertical	Eddy convergence
43°N										
Ice Age II	2	<0.01	−1.34	0.22	0.35	0.40	0.27	<0.01	0.12	0.06
Ice Age I	2	<0.01	−1.40	0.23	0.33	0.46	0.26	−0.02	0.11	−0.06
Current	5	<0.01	−1.43	0.24	0.22	0.57	0.16	0.00	0.30	−0.13
2 × CO_2	3	<0.01	−1.51	0.25	0.16	0.67	0.16	<0.01	0.19	0.03
Mesozoic	4	<0.01	−1.50	0.25	0.22	0.83	0.12	<0.01	0.24	−0.13
51°N										
Ice Age II	2	<0.01	−1.23	0.14	0.18	0.18	0.25	<0.01	0.10	0.25
Ice Age I	0	<0.01	−1.29	0.14	0.18	0.22	0.28	<0.01	0.00	0.32
Current	−2	<0.01	−1.35	0.16	0.17	0.41	0.24	0.00	−0.10	0.40
2 × CO_2	−2	<0.01	−1.44	0.16	0.13	0.53	0.25	<0.01	−0.12	0.36
Mesozoic	2	<0.01	−1.46	0.16	0.18	0.67	0.19	<0.01	0.12	0.08

extent of the subsidence. The effect in this model is to limit the change in Hadley cell poleward extent. The moist convective heat release (Fig. 5b) and solar radiation absorption (Fig. 4c) have similar gradients at low latitudes in four of the runs. As discussed by Rind and Rossow (1984), this helps explain why their Hadley cell intensities are similar.

The Mesozoic experiment does show a significantly different circulation cell pattern. The Hadley cell has two regions of peak intensity, with one shifted southward from that of the other experiments, and broken up by a region of downward vertical velocities at the equator. The increased intensity of the Southern Hemisphere peak is associated with the large latitudinal gradient in latent heat release between 12°S and the equator (Fig. 2a). The equatorial region of descent is apparently associated with the slightly cooler sea surface temperatures prescribed for the equatorial region (Fig. 1b), and corresponds to the location of minimum precipitation (Fig. 2a), minimum high cloud cover (Fig. 3b) and weaker convection (Figs. 5b, 5c). This run emphasizes the importance of the low-latitude sea surface temperatures in influencing the low-latitude circulation. Also, the maritime continent did not exist in the late Cretaceous; Stone and Chervin (1984) have emphasized the importance of this feature to the Hadley cell intensity, and ω is now small here.

- *Question 7:* Does the jet stream shift poleward as the climate warms?

If the high circulation index state does occur in warm climates, as the polar vortex shrinks, the jet stream will shift poleward. The model results, however, show no shift in jet stream position (Fig. 7a). The strongest winds occur at 31°N in all cases. There is also nothing systematic about changes in the jet stream intensity, as the doubled CO_2 climate has the greatest velocity, and the Mesozoic the smallest. The difference in velocities is only marginally significant (Table 2). If one considers the latitudinal gradient around the jet stream maximum there is some indication that ice-age westerlies are shifted slightly poleward in the Northern Hemisphere (as there was a slight expansion of the ice age Hadley circulation). The relative invariance of the jet stream also occurred in ice age experiments with the NCAR GCM (Williams and Barry, 1975).

The zonally averaged zonal momentum equation can be written:

$$\frac{\partial \bar{u}}{\partial t} = \bar{X} + \left[-\frac{\partial(\bar{u}\cos\phi)}{a\cos\phi\partial\phi}\bar{v} - \frac{\partial \bar{u}}{\partial p}\bar{\omega} \right] + \left[-\frac{\partial(\overline{u'v'}\cos^2\phi)}{a\cos^2\phi\partial\phi} - \frac{\partial(\overline{u'\omega'})}{\partial p} \right] + f\bar{v}, \quad (3)$$

where f is the Coriolis parameter, and $\bar{X}$ is any zonal mean nonconservative force, at the jet stream level in the model represented only by the change associated with momentum mixing by convection. The first bracketed term is the momentum change associated with the mean circulation, the second bracketed term is the momentum convergence by eddies, and the last term the effect of the Coriolis force on the meridional wind.

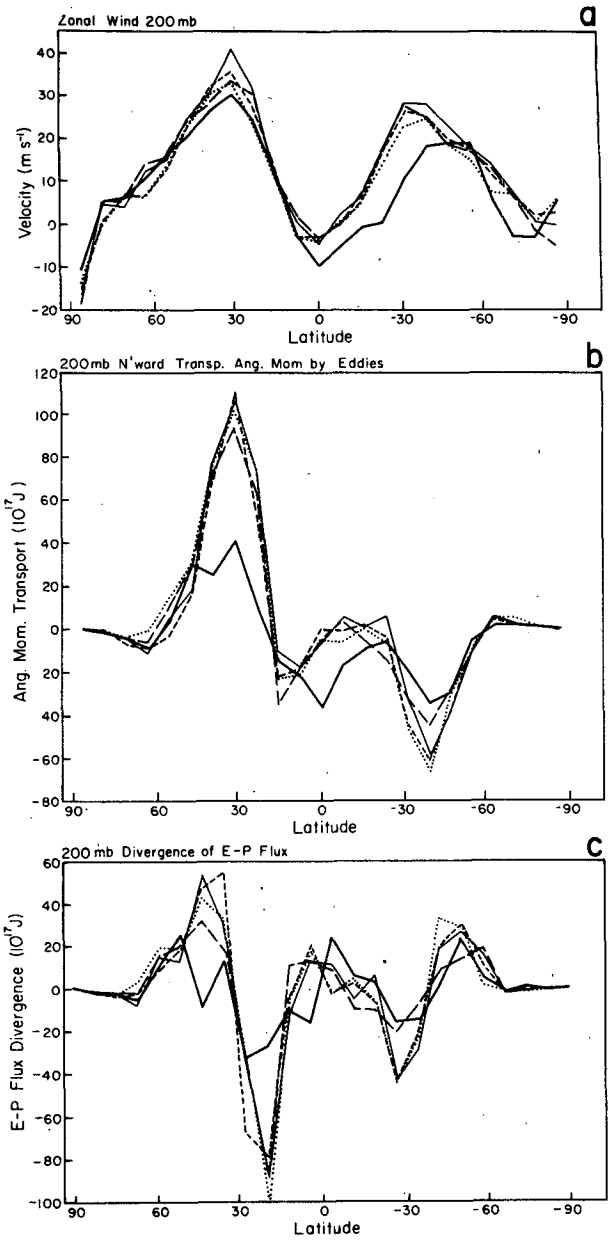

FIG. 7. As in Fig. 1 for (a) zonal wind at 200 mb; (b) 200 mb northward transport of angular momentum by eddies [shown divided by the length scale corresponding to the latitude grid spacing of 7.8°; to reproduce the customary units of $m^2\ s^{-2}$, multiply by this value in m, and divide by the moment arm ($a\cos\phi$) and by the mass of the layer, which has a pressure thickness of 150 mb]; (c) 200 mb divergence of Eliassen–Palm flux (to reproduce the customary units of $m\ s^{-2}$, divide by the moment arm and the pressure thickness of the layer). This presentation allows the eddy momentum flux convergence to be calculated by simply subtracting one latitude value from the next, with the result in the same units as for the E-P flux divergence.

For the 200 mb level the eddy transport of angular momentum is shown in Fig. 7b, while the balance from the different terms in Eq. (3) is given in Table 6, for both 31°N and 39°N. The balance cannot be calculated exactly because the convergences have to be interpolated to these latitudes (due to the arrangement of the winds on the grid). This introduces uncertainty especially in the convergence associated with mean circulation, since it is the result of large differences between horizontal and vertical transports. Nevertheless, it can be seen that the left-hand side of the equation in midwinter is small in magnitude, while the terms on the right-hand side are all of the same order. At 31°N the eddies remove momentum from the jet, as expected in a basically baroclinic atmosphere. The weakest divergences occur in the warm climates; however, in these climates, convection, which mixes momentum in the model, is making up the difference by removing more momentum. (Convective penetration is higher, Fig. 5c.) Again, there is compensation, here between eddy processes and convection.

At 39°N, the eddy convergences are weakest in the Mesozoic, but now there is compensation between the eddies and the mean circulation, an example of the tendency implied by the nonacceleration theorem (Charney and Drazin, 1961; Andrews and McIntyre, 1976). Alternatively, one can calculate the Eliassen–Palm flux divergences (Eliassen and Palm, 1961; Andrews and McIntyre, 1978). The differences between the Mesozoic and the other experiments still exist at this latitude (Fig. 7c). At the same time the eddies are producing momentum convergences, they are also setting up an indirect diabatic circulation through a latent heat release gradient (Fig. 2a, across midlatitudes). When acted upon by the Coriolis force, this indirect circulation will decelerate upper-level winds. Both of these eddy effects are weakest in the Mesozoic, and the result is to limit the change between different climate experiments.

d. Eddy energy

• *Question 8:* Is there greater baroclinic energy generation as climate cools?

In colder climates, the expected high-latitude amplification should lead to greater temperature gradients. In addition, the appearance of glaciers on land may well intensify the land–ocean temperature contrast. Colder climates thus should have increased available potential energy (APE), which might then be expected to lead to increased baroclinic energy generation following the cycle of zonal APE (ZAPE) → eddy APE (EAPE) → eddy kinetic energy (EKE).

The APE does increase systematically in the model as the climate cools (Table 1) at least in the Northern Hemisphere. Approximately two-thirds of the differences between the extreme climates is due to ZAPE changes, i.e., latitudinal temperature gradient effects. The latitudinal temperature gradient for a level slightly below the midtroposphere is shown in Fig. 8a, while the zonal average of the topography is given in Fig. 8b. Note that the warmest climate (Mesozoic) has both the smallest latitudinal temperature gradients and the smoothest topography, while both factors are greatest in the ice age experiments.

The baroclinic generation term may be calculated, for the EAPE → EKE part of the cycle as

$$G = -\overline{\omega'\alpha'}, \tag{4}$$

where α is the specific volume. The model results show baroclinic energy generation does increase as the climate cools. The latitudinal distribution of G for the 633 mb level (Fig. 8c) appears to emphasize the importance of both the latitudinal temperature gradient and topography. The ice age peak at 27°N results from the contrast between the cold air coming off the ice fields and the warm subtropical oceans. Even the summer hemisphere midlatitudes experience systematic, though small, increases.

The EAPE → EKE and ZKE → EKE transfers for the Northern Hemisphere (Table 7) show that the colder climates transfer more kinetic energy from eddies to the zonal mean, while in the Mesozoic the eddies actually gain energy from the zonal mean.

• *Question 9:* Does the eddy energy increase in colder climates, and how is this increase partitioned between stationary and transient waves?

A cold climate increase in the latitudinal temperature gradient is generally expected to result in increased eddy activity. However, the partitioning of this increase is unknown. Baroclinic transfer by itself should increase

TABLE 6. Momentum balance at 200 mb in units of 10^{-5} m s^{-2} at 31° and 39°N.

	31°N					39°N				
Experiment	$\frac{\partial u}{\partial t}$	Δ Moist convection	Δ Mean circulation	Δ Eddy	$f\bar{v}$	$\frac{\partial u}{\partial t}$	Δ Moist convection	Δ Mean circulation	Δ Eddy	$f\bar{v}$
Ice Age II	<0.1	−0.4	1.1	−1.7	2.3	<0.1	−0.2	0.4	2.4	−1.0
Ice Age I	<0.1	−0.6	1.3	−2.0	3.2	<0.1	−0.4	0.6	2.9	−1.6
Current	<0.1	−0.4	2.7	−1.2	1.1	<0.1	−0.2	0.6	1.8	−1.3
2 × CO_2	<0.1	−0.8	1.7	−1.0	1.4	<0.1	−0.4	−0.6	3.8	−2.2
Mesozoic	<0.1	−1.5	2.8	−1.0	2.8	<0.1	−0.6	1.0	0.5	0.1

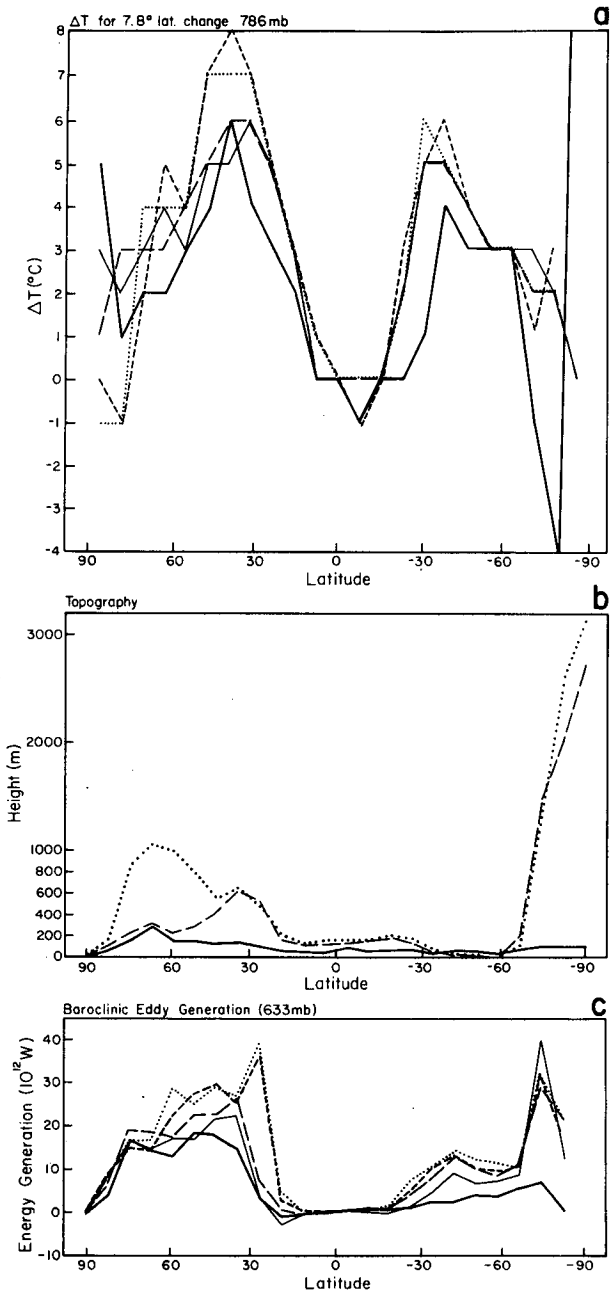

FIG. 8. As in Fig. 1 for (a) temperature gradient at 786 mb between one latitude and the next latitude 7.8° poleward; (b) topography (averaged over land and ocean); (c) baroclinic eddy generation at 633 mb ($-\omega'\alpha'$).

both stationary and transient waves, while increased wind speed, topography, ocean–land contrast might be expected to amplify the stationary component. Furthermore, modeling studies have shown that with reduced topography and stationary waves, transient waves increase (Manabe and Terpestra, 1974), and observations indicate that the effect of transient wave sensible heat fluxes is to diminish the stationary wave APE (Lau, 1979). Given these potential interactions, it is hard to establish a priori what will happen as climate changes.

Model results show that the eddy energy definitely increases in colder climates (Fig. 9a). Also, the global average transient eddy energy (defined for the monthly time scale) is about 73% of the total eddy energy in every climate (Table 1), a fairly remarkable result. This is not true at each latitude; for example, at 31°N, the stationary eddy energy (Fig. 9c) represents 40% of the total in the ice age experiments, and only 30% in the Mesozoic. Nevertheless, to first order we might conclude that the eddy energy retains the same ratio of stationary to transient energy in the various climates. To some extent this may be due to the coincidence of the warmest climate having both the smallest latitudinal temperature gradient and the smoothest topography, but as noted by Stone (1977), the ratio of stationary to transient eddy energy is similar in Northern Hemisphere winter and summer.

Transient eddy energy (Fig. 9b) seems to increase most at lower midlatitudes, and both transient eddy kinetic energy and baroclinic conversion shift southward in the Northern Hemisphere as climate cools. In contrast, the stationary eddy energy changes also extend to higher latitudes. This could have been expected given the influence of both topography and baroclinicity on stationary eddies. The runs with similar topography have somewhat similar stationary eddy energy, but the transient eddy energy is significantly different between the current and doubled CO_2 climates. Note also that the lack of topography maximum at midlatitudes in the Mesozoic (Fig. 8b) correlates with the lack of stationary eddy kinetic energy maximum at midlatitudes.

• *Question 10:* Does long wave energy increase proportional to short wave energy as climate cools, and how is any change partitioned into stationary and transient components?

As most historical climate changes are known from observations at a few stations with narrow longitudinal extent (e.g., Little Ice Age in Europe), it is often not clear whether they represent global changes or are associated more with changes in the longitudes of long wave troughs and ridges. A change in these longitudes may imply a change in Rossby wave length, i.e., a shift in the long wave energy spectrum. Furthermore, changes in long wave generation as the climate warms have implications for changes in stratospheric dynamics as carbon dioxide–induced warming occurs.

In analyses of baroclinic instability such as that of Green (1960), a stronger latitudinal temperature gradient shifts the region of maximum instability to longer wavelengths. If latitudinal temperature gradients increase in colder climates, baroclinicity should favor long wavelengths. Saltzman (1970) indicates the importance of baroclinic APE → EKE energy conversions in generating long waves in the atmosphere. How any change with climate would be partitioned between stationary and transient components is uncertain.

The model results show greater long wave energy in

TABLE 7. Baroclinic and barotropic conversions for the Northern Hemisphere in units of W m^{-2}.

	Ice Age II	Ice Age I	Current	$2 \times CO_2$	Mesozoic
EAPE → EKE	3.3	3.1	2.4	2.1	1.4
EKE → ZKE	0.78	0.67	0.20	0.27	−0.12

the colder climates (Fig. 10a). The energy spectrum is determined by Fourier analysis of the zonal and meridional wind fields. For wavenumbers 1 and 2 (of primary importance for the stratosphere), the change occurs in both the stationary waves (Fig. 10c) and the transient waves (Fig. 10b). The increased long wave energy is arising because of increased baroclinic conversion: the generation by the pressure gradient force for wavenumbers 1–4 for the Northern Hemisphere troposphere increases systematically from 0.09 W m^{-2} in the Mesozoic to 0.36 W m^{-2} in the ice age experiments, while the nonlinear conversion to wavenumbers 1–4 from other wavenumbers (including the zonal mean) decreases from 0.3 W m^{-2} in the Mesozoic to −0.13 W m^{-2} (exporting energy) in the ice age runs. The current climate and doubled CO_2 climate are again intermediate for both energy transfers. This part of the spectrum follows the general trend for all wavenumbers (Table 7).

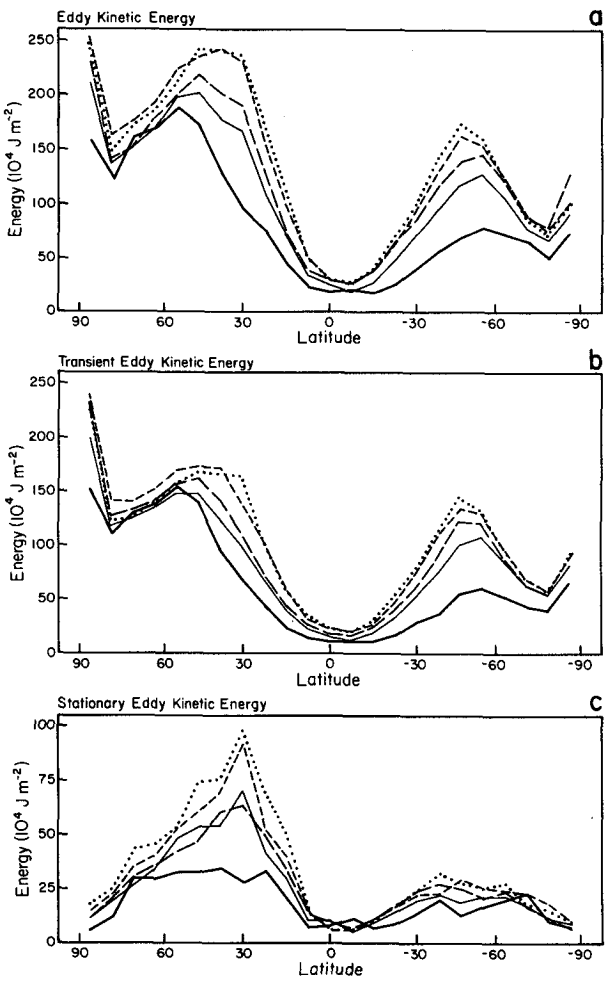

FIG. 9. As in Fig. 1 for (a) eddy kinetic energy; (b) transient eddy kinetic energy; (c) stationary eddy kinetic energy; stationary being defined over the time scale of one month. To reproduce the customary units of m^2 s^{-2} multiply by the area of the latitude circle, and divide by the moment arm and the mass of the atmosphere. All values are vertically integrated between the surface and 10 mb.

• *Question 11:* How do lapse rates change as the climate changes?

Stone (1978) argued that the lapse rate at midlatitudes satisfies a simple baroclinic adjustment hypothesis. The horizontal and vertical lapse rates are connected because a greater latitudinal temperature gradient should lead to the development of eddies with longer wavelengths; the longer wavelengths make possible greater vertical heat advection reducing the vertical lapse rate. Northern Hemisphere observations (Stone and Carlson, 1978) indicate that vertical lapse rates at midlatitudes of the Northern Hemisphere do appear to maintain the critical baroclinic instability values. The observations also indicate that low-latitude lapse rates are close to the moist adiabatic values. However, ice age terrestrial and oceanic evidence can be consistent only if the ice age low-latitude lapse rate departed substantially from the moist adiabatic (Webster and Streten, 1978; Rind and Peteet, 1985).

The global average value of the lapse rate remains relatively constant in the different experiments (Table 1). The lapse rates decrease at low latitudes in warmer climates (Fig. 11a), and increase at mid- and upper-latitudes. To understand this result, we can compare the value from each experiment with the moist adiabatic value, and also with the critical "dynamic" lapse rate determined from Stone's simplified baroclinic adjustment hypothesis (Figs. 12b–f). The critical dynamic lapse rate is calculated from the relation

$$\gamma_c = \gamma_{\text{dry adiabatic}} + \frac{\tan\phi}{H}\frac{\partial T}{\partial \phi}, \qquad (5)$$

where H and T are the mass-weighted scale height and temperature, respectively, of the troposphere.

At low latitudes, the lapse rate is near the moist adiabatic value in all the experiments, although it remains close for a wider range of latitudes as the climate warms. For example, in Ice Age II, it is very close to the moist adiabatic from 12°N to 20°S, while in the Mesozoic it is as close from 27°N to 35°S. As the climate warms, convection becomes more important in determining the full surface to 200 mb tropospheric lapse rate in the subtropics (Figs. 5b, 5c). With a warmer climate

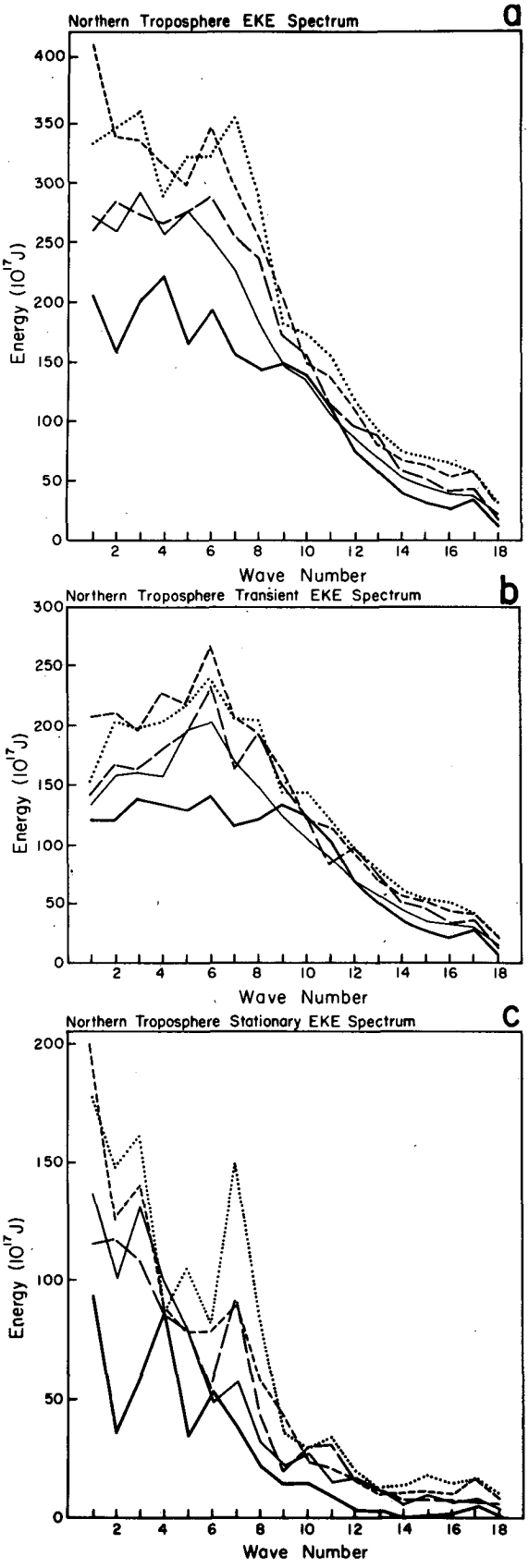

the moist adiabatic lapse rate decreases as the saturated air can hold more moisture; this explains the decreased lapse rates at low latitudes for the warmer climates. We should also note that this model does not use a moist adiabatic adjustment scheme for convection; the model's convective scheme tends to overstabilize by including compensatory subsidence of dry air (Hansen et al., 1983a), so the low-latitude temperature profile is not being continually forced to reproduce the moist adiabatic profile by the convective parameterization.

At midlatitudes there are two processes working to increase the lapse rate in the warmer climates. Vertical eddy transports produce energy divergence at 900 mb and convergence at 300 mb. With weaker and shallower eddies in warmer climates, this effect decreases. Moist convection tends to increase the lapse rate at these latitudes. In the warmer climates, penetrating moist convection is more abundant and this effect will be stronger. At mid- and upper-latitudes the figures show that the lapse rate increases as climate warms, and is fairly close to the critical dynamic value. The question is: Is this a reflection of the baroclinic adjustment parameterization, i.e., are the eddies responsible for the changes between climates, or is it more a reflection of changes in convection?

The results show that the energy gain at 300 mb relative to 900 mb due to eddies plus convection at 40°N is about 73×10^{13} W during the ice ages, and only about 10×10^{13} W in the Mesozoic, which is why the lapse rate increases in the Mesozoic. The change in vertical eddy transports accounts for 83% of this difference. Thus we conclude that the primary reason for the increased midlatitude lapse rate in the warmer climates is the change in vertical eddy transports, a conclusion which agrees with the results of Held (1976) who varied the solar constant in a two-level primitive equation model. The reasonable agreement with Stone's parameterization in the different climates is thus more than fortuitous, although admittedly the agreement is not perfect. In the warmer climates, with less snow and ice to stabilize the lower atmosphere at high latitudes, the applicability of baroclinic adjustment seems to extend further north. In the summer hemisphere baroclinicity is decreased so baroclinic adjustment is less important, especially in the warmer climates, and its region of applicability is more narrow.

e. Energy transports

• *Question 12:* How do the eddy energy transports change as climate changes?

Eddies transport sensible heat, latent heat and geopotential energy, as well as small amounts of kinetic

FIG. 10. As in Fig. 1 for northern troposphere (surface to 200 mb) eddy kinetic energy as a function of wavenumber. (a) Total eddy kinetic energy; (b) transient eddy kinetic energy; (c) stationary eddy kinetic energy.

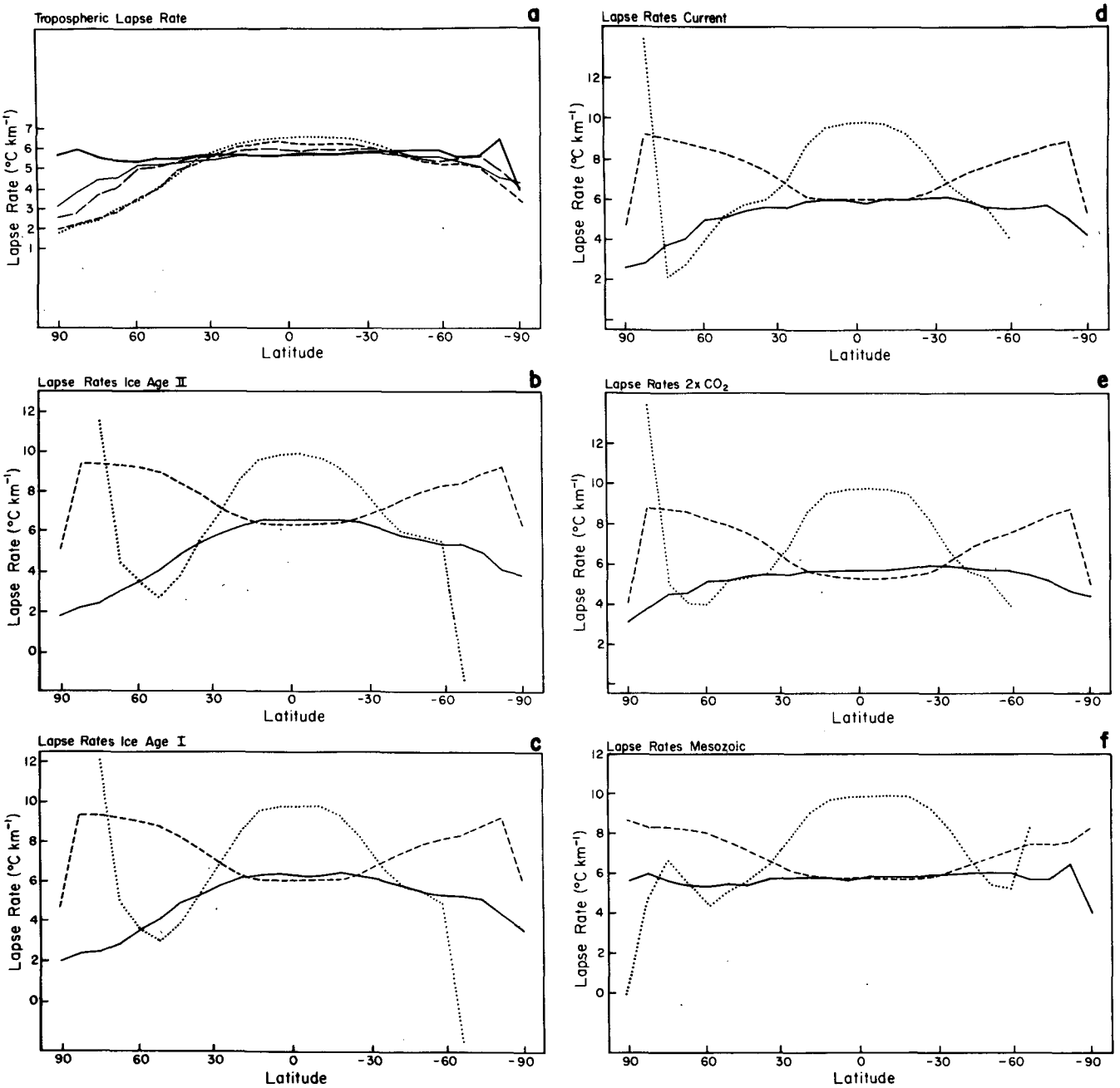

FIG. 11. As in Fig. 1 for (a) tropospheric lapse rates, calculated from the surface through 200 mb; (b)–(f) lapse rates for the individual experiments, with the solid line representing the actual lapse rate, the dashed line the moist adiabatic lapse rate, and the dotted line the critical dynamic (baroclinic adjustment) lapse rate: (b) Ice Age II; (c) Ice Age I; (d) current climate; (e) doubled CO_2; (f) Mesozoic.

energy. In colder climates, with greater eddy energy and larger latitudinal temperature gradients, the eddy sensible heat transport should be larger. Observations of the seasonal variations confirm this assumption, for both stationary and transient waves (Stone and Miller, 1980). The model results (Table 1, Fig. 12a) also show increased eddy sensible heat transports as climate cools, but the difference is mostly in the stationary eddy transports (Figs. 12b, c). Note also that the peak eddy heat transport is 10° latitude poleward of the peak temperature gradient (Fig. 8a), in agreement with observations discussed by van Loon (1979).

The variation of eddy latent heat transport with climate change is more difficult to predict. As climate warms eddy energy may decrease, but atmospheric moisture should increase. The model results show that

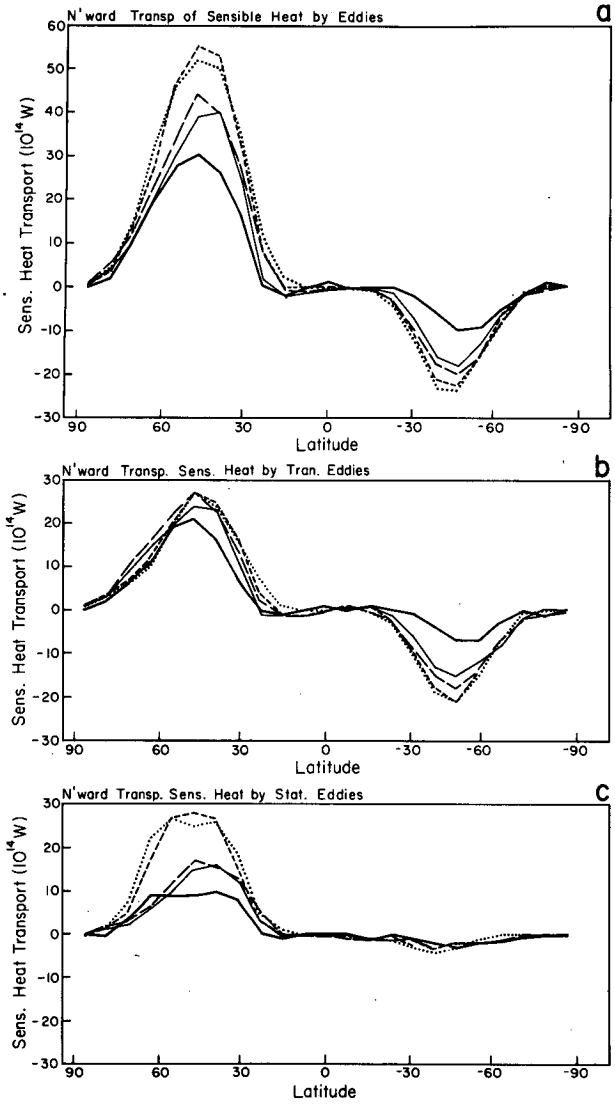

FIG. 12. As in Fig. 1 for (a) northward transport of sensible heat by eddies; (b) northward transport of sensible heat by transient eddies; (c) northward transport of sensible heat by stationary eddies. To reproduce the customary units of °C m s^{-1} divide by the specific heat at constant pressure, by the density, and by the area of the latitude-height plane. All values vertically integrated between the surface and 10 mb.

there is little systematic change in latent heat transport among the different climates (Fig. 13a). The warmest climates have slightly more northward transport poleward of 45°N, while south of 30°N the doubled CO_2 climate has the greatest poleward transport with the Mesozoic having the least. The results of both competing effects are seen; the ice age climates have less evaporation (Fig. 2b) but more eddy energy (Fig. 9a) than the others, and the reverse holds true for the warmer climates. The difference between the doubled CO_2 and Mesozoic climates results from their having similar evaporation while the Mesozoic has considerably less eddy energy. The doubled CO_2 climate has warmer low-latitude temperatures, which increases equatorial evaporation; it has cooler high-latitude temperatures, which allows for a larger latitudinal temperature gradient. Together with increased topography, this helps produce greater eddy energy.

The vertically integrated northward eddy transport of static energy is basically the sum of the sensible heat transport (Fig. 12a) and the latent heat transport (Fig. 13a) since the vertical integral of eddy geopotential energy transport is small. The eddy energy transport (Fig. 13b) increases in the colder climates due to the increased sensible heat flux since the latent heat flux is similar.

• *Question 13:* Do the eddies have a greater effect on the zonal mean circulation as the climate cools?

While eddy transports did increase somewhat in the colder climates, the eddy influence on the mean fields depends on the deviation from the nonacceleration criteria—transience and dissipation, or other diabatic effects (Charney and Drazin, 1961; Andrews and

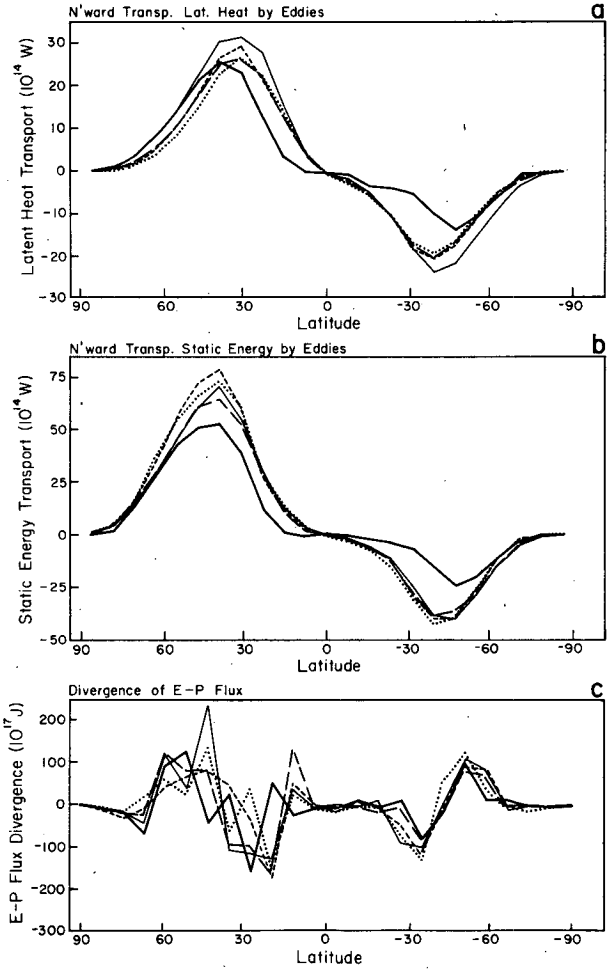

FIG. 13. As in Fig. 1 for (a) northward transport of latent heat by eddies; (b) northward transport of moist static energy by eddies; (c) divergence of the Eliassen–Palm flux. All values vertically integrated between the surface and 10 mb.

McIntyre, 1976). Much of the eddy transports of heat and momentum act to compensate one another, leaving the mean field unchanged.

The model results show no clear indication that eddies are influencing the zonal mean circulation to a greater degree in the cold climates. The vertically integrated divergence of the Eliassen–Palm flux (Fig. 14c) is "noisy" as might be expected from the vertical integration procedure which adds the midlatitude positive divergences at low and high altitudes with middle troposphere convergences (in qualitative agreement with Edmon et al., 1980, Fig. 5b). Nevertheless, a pattern emerges in both hemispheres: a tendency for acceleration of the mean flow from 40–60° latitude, and a deceleration at lower and higher latitudes. There is no obvious distinction in the magnitude of these effects among the different climates, perhaps due to the noise.

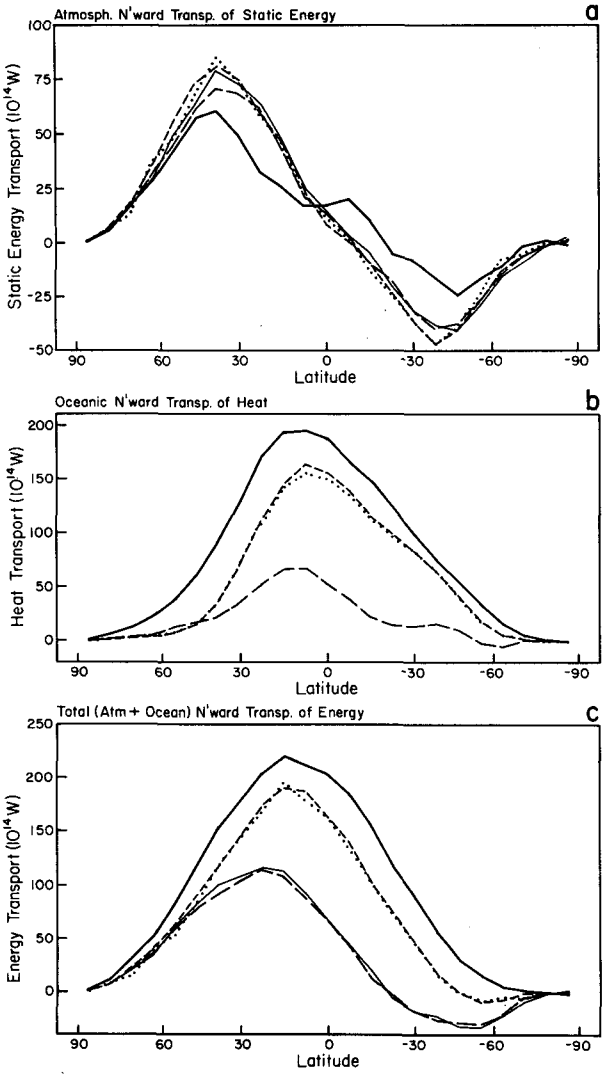

FIG. 14. As in Fig. 1 for (a) vertically integrated atmospheric (eddies plus mean circulation) northward transport of moist static energy; (b) implied oceanic northward heat transport; (c) atmosphere plus ocean total northward transport of energy.

The vertical integral of the E-P flux convergence is dominated by the vertical integral of eddy angular momentum convergences, whose values for the different experiments at a range of Northern Hemisphere latitudes can be compared with the vertically integrated zonal wind (Table 8). Again there is little systematic change in the eddy forcing. Differences of 10×10^{18} J, which do occur, should lead to zonal wind differences of 20 m s^{-1} over the month. The actual differences rarely exceed a few meters per second. Accompanying the increased eddy convergences are increases in frictional loss at the surface, which minimize their effect.

• *Question 14:* Does the total transport of energy increase as climate warms?

Could increased atmospheric transport be responsible for the high-latitude warmth apparently experienced during the Mesozoic? Does decreased atmospheric transport act as a positive feedback at high latitudes in ice age climates? The model results show that atmospheric transport of energy (Fig. 14a) is similar in all the experiments except the Mesozoic. The integrated poleward transport is within about 10% in the other four experiments (Table 1). In this GCM, differing transports, at least in winter, cannot provide the feedback needed to amplify warm or cold climates. Manabe and Wetherald (1980) for an annual average show decreased northward transport to high latitudes as the climate warms, until it gets very warm ($8 \times CO_2$). As noted earlier, this depends to some extent upon the high-latitude amplification—if the model shows only small temperature changes near the equator, as in the GFDL model, evaporation and latent heat transport increases will not be sufficient to overcome sensible heat transport decreases, and a negative feedback will result.

The total energy transport includes the transport implicit in the ocean due to the specification of sea surface temperatures in four of the five experiments. This ocean transport can be calculated as in Miller et al. (1983). Given the net heating of the ocean surface, corrected for any imbalance in the annual average radiation entering the ocean, we can deduce what energy convergence in each grid box is necessary to reproduce the specified sea surface temperature. From this we can calculate what transport would be necessary to produce those convergences. Miller et al. made the calculation for the annual average, which means they could assume no net heat storage in the vertical water column. As our result is for January we cannot make such an assumption, and, indeed, the convergence–divergence pattern for this month alone does not sum to zero. Instead we make the simple assumption that the net heat storage is partitioned everywhere proportional to the convergence, which alters the values by less than 10%. That accuracy is deemed sufficient for these purposes.

The average for the model's deduced current climate ocean transports (Fig. 14b) is in good agreement with observations (Hansen et al., 1983a). The doubled CO_2

TABLE 8. Vertically integrated eddy angular momentum convergence and zonal wind.

Experiment	67°N	59°N	51°N	43°N	35°N	27°N	20°N
			Eddy angular momentum convergence (10^{18} J)				
Ice Age II	2.5	6	8	19	−8	−8	−28
Ice Age I	0	6	13	12	2	−13	−20
Current	−1.0	14	13	10	−10	−16	−19
$2 \times CO_2$	−4.0	13	8	27	−13	−19	−13
Mesozoic	−6.0	11	14	−3	0	−20	6
			Vertically integrated zonal wind (m s^{-1})				
Ice Age II	3.6	5.1	9.5	14.0	16.4	13.7	6.2
Ice Age I	3.4	4.9	9.9	14.9	17.0	14.2	6.2
Current	5.7	9.0	11.6	14.5	15.0	14.7	7.0
$2 \times CO_2$	4.9	8.4	11.9	15.0	16.9	15.8	6.2
Mesozoic	5.2	8.1	10.8	12.3	12.8	10.4	5.4

experiment has the same transport as the current climate, explicitly. The ice age experiments need greatly increased northward heat transport from the summer hemisphere to produce the warm values shown by CLIMAP in the Northern Hemisphere subtropics, and this is true even if the temperatures everywhere are reduced by 2°C (as in Ice Age II). Frakes (1979) hypothesized that Mesozoic transports were indeed much higher, despite weaker ocean currents, because there would have been less vertical mixing, trapping solar radiational heating in the upper layers. Alternatively, the CO_2 value of the Mesozoic could have been a lot greater, perhaps a factor of 6 or more (Barron et al., 1981). This would have limited long wave cooling and changed the net heat loss at the ocean surface.

The total oceanic plus atmospheric energy transport (Fig. 15c) is dominated by the atmospheric transport north of 30°N except for the Mesozoic and by the oceanic in the subtropics of both hemispheres, similar to what is currently observed.

f. August results

We close this section with a brief discussion of the results for August. Selected global results for this month are shown in Table 1 and Table 4. Most of the trends are very similar to the January results. The major exception is that in the Southern Hemisphere the jet stream shifts poleward in the ice age experiments by 8° latitude, as does the region of minimum precipitation and maximum subsidence in the subtropics. This is contrary to expectation, although most paleoclimatic evidence is from the Northern Hemisphere. The magnitude of the Hadley circulation is fairly similar in all the experiments except the Mesozoic, as was true for the Northern Hemisphere in January. Gates (1976) and Williams et al. (1974) found weaker Hadley circulations for this month in their ice age simulations, while Manabe and Hahn (1977) produced a stronger circulation. As indicated in the discussion of the Northern Hemisphere January results, this too will depend on the sea surface temperature gradients, and several of the above studies used different ice age sea surface temperature data sets (older or pre-CLIMAP versions).

Despite the presence of glaciers, the ice age Northern Hemisphere in August has the dynamics of summer, with eddies and transports greatly reduced although still larger than for the warmer climates. The presence of ice reduces the solar radiation absorbed at 51°N by 11% compared to the current climate, which would help in maintaining the glaciers. The surface air temperature in the vicinity of the glaciers is generally near or below freezing, and the balance between pecipitation, evaporation and runoff is close to or greater than zero; i.e., the glaciers are not losing ice.

4. Discussion

One surprising result of these experiments is that despite the very diverse nature of the climates, many aspects of the zonal-average dynamics show little change. The Hadley cell, jet stream, and total atmospheric energy transport are similar in most of the runs. Rind and Rossow (1984) showed that drastic alterations in specific physical parameters will produce changes in the Hadley cell, but many complex feedback processes occurred. In these experiments, with less drastic alterations, the feedbacks produced compensations in the thermal (Table 5) and momentum (Table 6) fields, limiting the differences between climates.

One reason for the compensating nature of the feedbacks may be the similarity of the sea surface temperature and absorbed solar radiation gradients across midlatitudes in the winter hemispheres (Table 4; Fig. 4c). In four of the experiments ocean gradients are prescribed; the resulting latitudinal gradients of the vertically integrated air temperatures are also similar. The implication is that the ocean and solar gradients are controlling the tropospheric latitudinal temperature gradient; as warm and cold climates have different mechanisms for heating (Table 5), the types of processes (convection, eddies) differ, but the net effect is the same. Similarities in the midlatitude tropospheric tempera-

ture gradient and similarities in the total atmospheric transport (Fig. 14a) are presumably related as well.

The doubled CO_2 experiment generated its own sea surface temperature gradient, which turned out to be similar to the others (Table 4). Whether this gradient is a real property of the system, or at least the model, requires additional experiments. A 2% solar constant increase run also produced the same result (Hansen et al., 1984), as well as similar jet streams, Hadley cells, etc. If the sea surface temperature gradient or the vertically integrated atmospheric temperature gradient is a common feature, it may be related to the properties of the water molecule (specifically the Clausius–Clapeyron equation), as water vapor is a dominant factor in the thermal balance through cloud cover, greenhouse capacity and latent heat release when CO_2 is small.

The stationary to transient eddy energy had the same ratio in the different climates (Table 1). As noted, this is probably related at least in part to the coincidence of the coldest climates having both the largest topography and the greatest latitudinal temperature gradients. The differences in eddy sensible heat transports result primarily from changes in the stationary eddy transports (Fig. 12). While the eddy energy transports are slightly larger in colder climates, there are no obvious differences in the eddy effects on the zonal mean circulation (Fig. 13c, Table 8)—the eddy transport differences do not produce differences in the latitudinal temperature gradients.

Other conclusions are that lapse rates are moist convective at low latitudes and close to Stone's critical baroclinic lapse rate at midlatitudes in all the climates. Low-level and total clouds increase in colder climates, while high-level clouds decrease. Convection and cloud cover are highly parameterized processes, which raises the more general question: How valid are the model results? The relative invariances of the January Hadley cell, precipitation patterns and jet stream all depend upon balances, which result to some extent from the model's parameterizations. Furthermore, most of the conclusions depend crucially on the sea surface temperature prescriptions (or, in the case of doubled CO_2, prescribed transports). Are they consistent with the atmospheric forcing? The differences between the doubled CO_2 and Mesozoic climates underscore that warm climates will be very different depending on the sea surface temperature latitudinal gradient. The warm low- and subtropical-latitude ocean temperatures prescribed by CLIMAP influence many aspects of the cold climate generation. Where these results violate conclusions derived from interpretations of paleoclimate indicators, either the interpretations, the model, or the prescribed sea surface temperatures are inaccurate. View the individual answers, then, as coming from one GCM with a particular set of sea surface temperatures.

Acknowledgments. The help of many people in the production and presentation of these results is gratefully acknowledged. For the set-up and generation of the different climates, thanks go to J. Hansen, A. Lacis, R. Fairbridge, J. Kuhn, J. Flemming and H. Brooks; for the diagnostic output, G. Russell, R. Suozzo, R. Ruedy, and J. Lerner. Advice on the manuscript was given by T. Del Genio, W. Robinson, W. Rossow and R. Seager. J. Mendoza and L. Del Valle drafted the figures and the manuscript was typed by A. Calarco and J. Li. The climate modeling was supported by the NASA Climate Program managed by Dr. Robert Schiffer, and the doubled CO_2 work was supported by EPA, principally through the efforts of John Hoffman.

REFERENCES

Andrews, D. G., and M. E. McIntyre, 1976: Planetary waves in horizontal and vertical shear: The generalized Eliassen-Palm relation and the mean zonal acceleration. *J. Atmos. Sci.*, **33**, 2031–2048.

——, and ——, 1978: Generalized Eliassen-Palm and Charney-Drazin theorems for waves on axisymmetric mean flows in compressible atmosphere. *J. Atmos. Sci.*, **35**, 175–185.

Barron, E. J., C. G. A. Harrison, J. L. Sloan and W. W. Hay, 1981: Paleogeography, 180 million years ago to the present. *Eclogae Geol. Helv.*, **74**, 443–470.

——, and W. M. Washington, 1982a: Atmospheric circulation during warm geologic periods: Is the equator-to-pole surface-temperature gradient the controlling factor? *Geology*, **10**, 633–636.

——, and ——, 1982b: Cretaceous climate: A comparison of simulations with the geologic record. *Paleogeography, Paleoclimatology, Paleoecology*, **40**, 103–133.

——, and ——, 1984: The role of geographic variables in explaining paleoclimates: results from Cretaceous climate model sensitivity studies. *J. Geophys. Res.*, **89**, 1267–1279.

Berger, A. L., 1978: Long-term variations of daily insolation and quaternary climatic changes. *J. Atmos. Sci.*, **35**, 2362–2367.

Budyko, M., 1974: Climate modification techniques. *Meteor. and Hydr.*, **2**, 110–122 (English translation).

Charney, D., and P. Drazin, 1961: Propagation of planetary-scale disturbances from the lower into the upper atmosphere. *J. Geophys. Res.*, **66**, 83–109.

Chervin, R. M., and L. M. Druyan, 1984: The influence of ocean surface temperature gradient and continentality on the Walker Circulation. Part I: Prescribed tropical changes. *Mon. Wea. Rev.*, **112**, 1510–1523.

CLIMAP Project Members (A. McIntyre, project leader), 1981: Seasonal reconstruction of the earth's surface at the last glacial maximum. Geol. Soc. Amer., Map and Chart Series, No. 36.

Crutcher, H., and J. Meserve, 1970: *Selected Level Heights, Temperatures and Dew Points for the Northern Hemisphere.* NAVAIR 50-1C-52, 424 pp. [U.S. Govt. Printing Office.]

Druyan, L., 1982. Studies of the Indian summer monsoon with a coarse-mesh general circulation model. Part I. *J. Climatology*, **2**, 347–355.

Edmon, H. J. Jr., B. J. Hoskins and M. E. McIntyre, 1980: Eliassen-Palm cross sections in the troposphere. *J. Atmos. Sci.*, **37**, 2600–2616.

Eliassen, A., and E. Palm, 1961: On the transfer of energy in stationary mountain waves. *Geofys. Publ.*, **22**, 1–23.

Fleming, J., 1983: Late Cretaceous climate simulation using GISS model II general circulation model. Summer Institute Research Project, Summer Institute for Planets and Climate, sponsored by Columbia University in conjunction with NASA GISS, 69–87. [Available from D. Rind.]

Frakes, L. A., 1979: *Climates Throughout Geologic Time.* Elsevier, 310 pp.

Gates, W. L., 1976: The numerical simulation of ice-age climate with a global general circulation model. *J. Atmos. Sci.*, **33**, 1844–1873.

Green, J. S. A., 1960: A problem in baroclinic instability. *Quart. J. Roy. Meteor. Soc.*, **86**, 237–251.

Hansen, J., G. Russell, D. Rind, P. Stone, A. Lacis, S. Ledeff, R. Reudy and L. Travis, 1983a: Efficient three-dimensional global models for climate studies: Models I and II. *Mon. Wea. Rev.*, **111**, 609–662.

——, D. Johnson, A. Lacis, S. Lebedeff, P. Lee, D. Rind and G. Russell, 1983b: Climatic effects of atmospheric carbon dioxide. *Science*, **220**, 873–875.

——, A. Lacis, D. Rind, G. Russell, P. Stone, I. Fung, R. Ruedy and J. Lerner, 1984: Climate sensitivity: analysis of feedback mechanism. In *Climate Processes and Climate Sensitivity*, editors J. E. Hansen and T. Takahashi, American Geophysical Union, Washington, D.C., 130–163.

Held, I., 1976: The tropospheric lapse rate and climate sensitivity. Ph.D. thesis, Princeton University, 217 pp. [Available from University Microfilms International, Ann Arbor.]

——, and A. Y. Hou, 1980: Nonlinear axially symmetric circulations in a nearly inviscid atmosphere. *J. Atmos. Sci.*, **37**, 515–533.

Henderson-Sellers, A., and V. Gornitz, 1984: Tropical deforestation and climate change. *Climatic Change*, **6**, 231–257.

Kuhn, J. A., 1982: Possible climatic effects of a large meteorite incident upon the earth 65 million years ago. *J. Undergrad. Res. in Phys.*, **1**, 11–20.

Kutzbach, J. E., and P. J. Guetter, 1984: Sensitivity of late-glacial and Holocene climates to the combined effects of orbital parameter changes and lower boundary condition changes: "snapshot" simulations with a general circulation model for 13, 9 and 6 ka BP. *Ann. Glaciology*, **5**, 85–87.

Lamb, H. H., 1972: *Climate: Present, Past and Future. Fundamentals and Climate Now*, Vol. 1, Metheun, 631 pp.

Lau, N-C., 1979: The observed structure of tropospheric stationary waves and the local balances of vorticity and heat. *J. Atmos. Sci.*, **36**, 996–1016.

——, and A. H. Oort, 1981: A comparative study of observed Northern Hemisphere circulation statistics based on GFDL and NMC analyses. Part 1: The time-mean fields. *Mon. Wea. Rev.*, **109**, 1380–1403.

Lindzen, R., A. Hou and B. Farrell, 1982: The role of convective model choice in calculating the climatic impact of doubled CO_2. *J. Atmos. Sci.*, **39**, 1189–1205.

London, J., 1957: A study of the atmospheric heat balance. New York University Rep., AFCRC-TR-57-287, ASTIA no. 117227, 99 pp.

Manabe, S., and R. T. Wetherald, 1967: Thermal equilibrium of the atmosphere with a given distribution of relative humidity. *J. Atmos. Sci.*, **24**, 241–259.

——, and T. B. Terpstra, 1974: The effects of mountains on the general circulation of the atmosphere as identified by numerical experiments. *J. Atmos. Sci.*, **31**, 3–42.

——, and R. T. Wetherald, 1975: The effects of doubling the CO_2 concentrations on the climate of a general circulation model. *J. Atmos. Sci.*, **32**, 3–15.

——, and D. G. Hahn, 1977: Simulation of the tropical climate of an ice age. *J. Geophys. Res.*, **82**, 3889–3911.

——, and R. J. Stouffer, 1980: Sensitivity of a global climate model to an increase of CO_2 concentration in the atmosphere. *J. Geophys. Res.*, **85**, 5529–5554.

——, and R. T. Wetherald, 1980: On the distribution of climate change resulting from and increase of CO_2 content of the atmosphere. *J. Atmos. Sci.*, **37**, 99–118.

——, and A. J. Broccoli, 1984: Ice-age climate and continental ice sheets: Some experiments with a general circulation model. *Ann. Glaciology*, **5**, 100–105.

Manabe, S., R. T. Wetherald and R. J. Stouffer, 1975: Summer dryness due to an increase of atmospheric CO_2 concentration. *Climatic Change*, **3**, 347–386.

Miller, J. R., G. L. Russell and L-C. Tsang, 1983: Annual oceanic heat transports from an atmospheric model. *Dyn. Atm. Oceans*, **7**, 95–109.

Newell, R., and T. Dopplick, 1979: Questions concerning the possible influence of anthropogenic CO_2 on atmospheric temperature. *J. Appl. Meteor.*, **18**, 822–825.

——, and S. Gould-Stewart, 1981: A stratospheric fountain? *J. Atmos. Sci.*, **38**, 2789–2796.

Oort, A. H., and T. P. Peixoto, 1983: Global angular momentum and energy balance requirements from observations. *Adv. Geophys.*, **25**, 355–490.

——, and E. Rasmusson, 1971: *Atmospheric Circulation Statistics*. NOAA Prof. Pap. 5, U.S. Dept. of Commerce, 323 pp.

Rind, D., 1982: The influence of ground moisture conditions in North America on summer climate as modeled in the GISS GCM. *Mon. Wea. Rev.*, **110**, 1487–1494.

——, and W. Rossow, 1984: The effects of physical processes on the Hadley circulation. *J. Atmos. Sci.*, **41**, 479–507.

——, and D. Peteet, 1985: Terrestrial conditions at the last glacial maximum and CLIMAP sea-surface temperature estimates: Are they consistent? *Quart. Res.*, **24**, 1–22.

Roads, J., 1978: Relationships among fractional cloud cover, relative humidity and condensation in a simple wave model. *J. Atmos. Sci.*, **35**, 1450–1462.

Saltzman, B., 1970: Large-scale atmospheric energetics in the wavenumber domain. *Rev. Geophys. Space Physics*, **8**, 289–302.

Sarnthein, M., 1978: Sand deserts during Glacial maximum and climatic optimum. *Nature*, **272**, 43–46.

Schlesinger, M., 1984: Atmospheric general circulation model simulations of the modern Antarctic climate. Workshop on potential CO_2-induced changes in the environment of West Antarctica, National Research Council, National Academy of Sciences, 51 pp.

Schneider, S., W. Warren and R. Chervin, 1978: Cloudiness as a climatic feedback mechanism: Effects on cloud amounts of prescribed global and regional surface temperature changes in the NCAR GCM. *J. Atmos. Sci.*, **35**, 2207–2221.

Schutz, C., and W. Gates, 1971: Global climatic data for surface, 800 mb, 400 mb. Rep. R-915-ARPA, Rand Corp., 173 pp.

Stephens, G. L., G. G. Campbell and T. H. Vonder Haar, 1981: Earth radiation budgets. *J. Geophys. Res.*, **86**, 9739–9760.

Stone, P. H., 1977: Generation of atmospheric eddies. *Theory and Modeling of Ocean Eddies*, P. Rhines, Ed., U.S. Polymode Organizing Committee, Cambridge, MA, 22 pp.

——, 1978: Baroclinic adjustment. *J. Atmos. Sci.*, **35**, 561–571.

——, and J. H. Carlson, 1979: Atmospheric lapse rate regimes and their parameterization. *J. Atmos. Sci.*, **36**, 415–423.

——, and D. A. Miller, 1980: Empirical relations between seasonal changes in meridional temperature gradients and meridional fluxes of heat. *J. Atmos. Sci.*, **37**, 1708–1721.

——, and R. M. Chervin, 1984: The influence of ocean surface temperature gradient and continentality on the Walker circulation. Part II: Prescribed global changes. *Mon. Wea. Rev.*, **112**, 1524–1534.

Street, F. A., and A. T. Grove, 1979: Global maps of lake-level fluctuations since 30,000 yr B.P. *Quart. Res.*, **12**, 83–118.

van Loon, H., 1979: The association between latitudinal temperature gradient and eddy transport. Part I: Transport of heat in winter. *Mon. Wea. Rev.*, **107**, 525–534.

Washington, W., and G. Meehl, 1984: Seasonal cycle experiment on the climate sensitivity due to a doubling of CO_2 with an atmospheric general circulation model coupled to a simple mixed layer ocean model. *J. Geophys. Res.*, **89**, 9475–9503.

Webster, P., and N. Streten, 1978: Late Quaternary ice age climates of tropical Australasia, interpretation and reconstruction. *Quart. Res.*, **10**, 279–309.

Williams, J., and R. G. Barry, 1975: Ice Age experiments with the NCAR general circulation model, conditions in the vicinity of northern continental ice sheets. In *Climate of the Arctic*, G. Weller and S. A. Bowling, Eds., University of Alaska Press, 143–149.

——, R. G. Barry and W. M. Washington, 1974: Simulation of the atmospheric circulation using the NCAR global circulation model with ice age boundary conditions. *J. Appl. Meteor.*, **13**, 305–317.

Winstanley, D., 1973: Rainfall patterns and general atmospheric circulation. *Nature*, **245**, 190–194.